RESEARCH ARTICLE

Journal of **Applied Toxicology** WILEY

Methylglyoxal-induced neurotoxic effects in primary neuronal-like cells transdifferentiated from human mesenchymal stem cells: Impact of low concentrations

Teresa Coccini[1] 🔾 | Azzurra Schicchi[1] | Carlo Alessandro Locatelli[1] | Francesca Caloni[2] 🔾 | Sara Negri[3] | Elena Grignani[3] | Uliana De Simone[1]

[1]Laboratory of Clinical and Experimental Toxicology, and Pavia Poison Centre-National Toxicology Information Centre, Toxicology Unit, Istituti Clinici Scientifici Maugeri IRCCS, Pavia, Italy

[2]Dipartimento di Scienze e Politiche Ambientali (ESP), Università degli Studi di Milano, Milan, Italy

[3]Environmental Research Center, Istituti Clinici Scientifici Maugeri IRCCS, Pavia, Italy

Correspondence
Teresa Coccini, Laboratory of Clinical and Experimental Toxicology, and Pavia Poison Centre-National Toxicology Information Centre, Toxicology Unit, Istituti Clinici Scientifici Maugeri IRCCS, Pavia, Italy.
Email: teresa.coccini@icsmaugeri.it

Abstract

In the last decades, advanced glycation end-products (AGEs) have aroused the interest of the scientific community due to the increasing evidence of their involvement in many pathophysiological processes including various neurological disorders and cognitive decline age related. Methylglyoxal (MG) is one of the reactive dicarbonyl precursors of AGEs, mainly generated as a by-product of glycolysis, whose accumulation induces neurotoxicity. In our study, MG cytotoxicity was evaluated employing a human stem cell-derived model, namely, neuron-like cells (hNLCs) transdifferentiated from mesenchymal stem/stromal cells, which served as a source of *human based* species-specific "healthy" cells. MG increased ROS production and induced the first characteristic apoptotic hallmarks already at low concentrations (≥10 μM), decreased the cell growth (≥5–10 μM) and viability (≥25 μM), altered Glo-1 and Glo-2 enzymes (≥25 μM), and markedly affected the neuronal markers MAP-2 and NSE causing their loss at low MG concentrations (≥10 μM). Morphological alterations started at 100 μM, followed by even more marked effects and cell death after few hours (5 h) from 200 μM MG addition. Substantially, most effects occurred as low as 10 μM, concentration much lower than that reported from previous observations using different in vitro cell-based models (e.g., human neuroblastoma cell lines, primary animal cells, and human iPSCs). Remarkably, this low effective concentration approaches the level range measured in biological samples of pathological subjects. The use of a suitable cellular model, that is, human primary neurons, can provide an additional valuable tool, mimicking better the physiological and biochemical properties of brain cells, in order to evaluate the mechanistic basis of molecular and cellular alterations in CNS.

KEYWORDS
aging, glycotoxins, human mesenchymal stem cells, in vitro human cell-based testing, neurodegeneration, neurotoxicity

1 | INTRODUCTION

In the last decades, advanced glycation end-products (AGEs), also called "glycotoxins," have aroused the interest of the scientific community due to the increasing evidence of their involvement in many pathophysiological processes (i.e., diabetes) and various neurological disorders such as Alzheimer's disease (AD), Parkinson's disease (PD), schizophrenia, cognitive decline related to aging, and behavior-related disorders—pain, anxiety, and depression (Allaman et al., 2015; Beeri et al., 2011; Bhat et al., 2015; de Almeida et al., 2023; Twarda-Clapa et al., 2022). AGEs constitute a non-homogenous, chemically diverse group of compounds formed either exogeneously or endogenously on the course of various pathways in the human body (Twarda-Clapa et al., 2022). Methylglyoxal (MG) is one of the reactive dicarbonyl precursors of AGEs that can act as a typical glycating agent and is mainly generated as a by-product of glycolysis when the spontaneous degradation of glyceraldehyde 3-phosphate (GA3P) occurs and to a lesser extent as by-product of protein and fatty acid metabolism (Kold-Christensen & Johannsen, 2020). Therefore, as inevitably MG accumulates in all cells, its excess has been proposed to be highly deleterious (Rabbani & Thornalley, 2015). MG readily reacts with basic phospholipids and nucleotides, as well as amino acid residues of proteins, such as arginine, cysteine, and lysine, thus generating AGEs (Rabbani et al., 2016), which ultimately contribute to cellular damage, neuronal dysfunction, and impaired behavior (de Almeida et al., 2023; Kalapos, 2008; Schmitz et al., 2017; Szczepanik et al., 2020).

Considering the brain's high energy (i.e., glucose) requirements for maintaining neural cell functions and tight regulation of glucose metabolism, the main source of energy, essential for brain physiology, neuronal cells are those potentially most exposed to the toxic effects produced by the accumulation of MG, which can lead to augmented levels of AGEs (Manza et al., 2020; Yang et al., 2022).

Evidences indicate that the metabolic profile of neural cells as regards the glycolysis process is not homogeneous but instead occurs with a tendency that is greater in astrocytes compared to that observed in neurons (Allaman et al., 2015). These two types of neural cells have also different defense. In physiological situations, cells are protected against MG toxicity through the glyoxalase system, which includes two key metalloenzymes, Glyoxalase-1 (Glo-1) and Glyoxalase-2 (Glo-2), both of which use GSH as a co-factor. The glyoxalase system pathway metabolizes more than 99% MG under normal condition detoxifying/converting MG into d-lactic acid using GSH. This system, a ubiquitous enzymatic pathway and the main detoxifying system for MG, differs between astrocytes and neurons. Glo-1 and Glo-2 enzymes activities (with Glo-1 activity always substantially higher than that of Glo-2) are significantly higher in astrocytes compared to neurons and are such as to make neurons more vulnerable to the accumulation of MG and AGEs and, therefore, to the resulting toxicity. Again, higher GSH concentrations are found in astrocytes (Dringen, 2000) that, along with the higher Glo-1 and Glo-2 activities (Thornalley, 2008), indicate a more astrocyte efficiency on MG elimination.

MG can render neurons susceptible to AGE formation, a risk factor linked to the development of neurodegenerative disorders, at high level and can induce oxidative stress and cause irreversible loss of protein function, including protein cross-linking (Currais & Maher, 2012).

Consistent with a less active glyoxalase system, neurons are more vulnerable than astrocytes to MG toxicity, as exogenously added MG at concentrations between 250 and 800 μM is detrimental to neuronal viability in laboratory animals hippocampal, cortical, and primary sensory cortex cultures or in human neuroblastoma cells (Angeloni et al., 2015; Bélanger et al., 2011; de Arriba et al., 2007; di et al., 2004, 2008; Radu et al., 2012; Tseng et al., 2019), while concentrations up to 1 mM do not impact cellular integrity in astrocytic cultures or in rat C6 glioma cells (Bélanger et al., 2011; Hansen et al., 2012).

Direct comparison of MG toxicity in primary cultures of mouse cortical neurons and astrocytes evidenced a sixfold higher susceptibility toward MG toxicity in neurons compared to astrocytes (Bélanger et al., 2011). Even more strikingly, when mouse astrocytes and neurons were co-cultured, neurons were significantly protected from MG toxicity (added at concentrations of up to 2 mM) (Bélanger et al., 2011). Similarly, in a co-culture model of human astrocytes (D384 cell line) and neurons (SH-SY5Y cell line), the protection of neurons by astrocytes was remarked (De Simone et al., 2017), further highlighting the high capacity of astrocytes to detoxify extracellular sources of MG, protecting neurons in the process.

On the whole, the various in vitro studies reporting the neurotoxicity induced by MG and AGEs are carried out mainly using animal brain cells (i.e., primary or cell lines of astrocytes, cortex, hippocampus, and endothelial) or human neuroblastoma cells, such as SH-SY5Y (Angeloni et al., 2015; de Oliveira et al., 2021; He et al., 2022; Popelová et al., 2018; Qi et al., 2022; Strom et al., 2021; Tseng et al., 2019), SK-N-SH (Haddad et al., 2019), SK-N-MC (Suh et al., 2022), and M17 (Conti Mazza et al., 2022). In particular, in human neuroblastoma cells, treatment with MG leads to abnormal glucose metabolism and energy depletion (de Arriba et al., 2007), oxidative stress, and apoptosis (Angeloni et al., 2015; Dafre et al., 2017; de Oliveira et al., 2018; Jiang et al., 2016; Tseng et al., 2019) triggering neuronal damage commonly seen in PD and AD (Lai et al., 2022; Li et al., 2012; Xie et al., 2014).

This study is focused on the evaluation of the cytotoxic effects induced by MG applying an in vitro human primary cell-based model, namely, neuron-like cells (hNLCs) differentiated from the human umbilical cord lining membrane-derived mesenchymal stem/stromal cells.

Primary cells of human origin are strongly recommended as relevant alternative methods to predict toxicological profiles improving prevention, treatment, and public health in general. With the recent rapid development of stem cell (SC) technology, many studies are seeking to differentiate human SCs into specific cells of interest, and this approach is also pursued in the area of neurotoxicity testing (Kim et al., 2019; Masjosthusmann et al., 2018; Singh et al., 2016). One

type of SCs includes the "mesenchymal stem cells" (MSCs), multipotent SCs that exhibit numerous advantages, including the fact that they can be obtained in high yield from healthy human adult tissues, have the advantage over primary and immortalized cells of being capable of continuous, repeated self-renewal, and of forming large populations of stably differentiated cells representative of different tissues of human origin, including cerebral cells (e.g., neuronal and glial cells; Kim et al., 2019; Singh & Kashyap, 2016; Suma & Mohanan, 2015; Zakrzewski et al., 2019) and can be cultured with a minimal laboratory setup and without genetic manipulations. They can be easily obtained from the human umbilical cord with painless, non-invasive, and ethically acceptable collection procedure and be efficiently differentiated in vitro into cells of nonmesodermal origin, including hNLCs (Coccini et al., 2022; Cortés-Medina et al., 2019; Czarnecka et al., 2017; Hernández et al., 2020; Kil et al., 2016; Shahbazi et al., 2016; Shi et al., 2018), which can be used as a powerful tool for chemical neurotoxicological risk assessment in humans (Buzanska et al., 2009; Coccini et al., 2020; De Simone et al., 2020; Kashyap et al., 2015; Singh et al., 2016; Singh & Kashyap, 2016; Zychowicz et al., 2014).

These hNLCs, serving as a source of "healthy" cells (that are not immortalized or cancer-derived cell lines), species-specific, human based, have been employed to evaluate MG toxicity using a range of concentrations typically detected in the plasma of pathological subjects (Beeri et al., 2011; Haddad et al., 2019; Srikanth et al., 2013). Different functional and biochemical parameters that are potential toxicity targets of MG or MG-derived adducts, namely, mitochondrial function and membrane integrity, cell morphology and growth, nuclear apoptotic features and caspase-3/7 activity, glyoxalase activity, intracellular ROS, and typical neuronal markers, namely, MAP-2 (microtubule associated protein 2) a marker for the cell body and neurites, and enolase–NSE (Neuron-Specific Enolase) enzyme of the glycolytic pathway expressed predominantly in neurons, have been evaluated. Parallelly, the intra-cellular (cell lysate) and extra-cellular (medium) levels of free MG were also evaluated.

2 | MATERIALS AND METHODS

2.1 | Cell culture reagents and supplies

MSC growth medium 2 (Ready-to-use; PromoCell, Heidelberg, Germany), MSC neurogenic differentiation medium (Ready-to-use; PromoCell), human fibronectin solution (1 mg/ml; PromoCell), all cell culture reagents, and 96-well plates (black well/clear bottom plate; ThermoFisher Scientific, Milan, Italy) were purchased from Carlo Erba Reagents (Carlo Erba Reagents S.r.l., Cornaredo, Italy). Tissue culture flasks of 75 cm^2 with vented filter caps (Corning, Schnelldorf, Bavaria, Germany) were acquired from Merck Life Science S.r.l. (Milan, Italy). Accutase solution (DUTSCHER), 6- and 96-well plates (SPL), and Amicon ultra-0.5 centrifugal filter units (3 kDa MWCO, Millipore, Tullagreen, Carrigtwohill, County Cork, Ireland) were obtained from BioSigma S.p.A. (Cona, Italy).

2.2 | Chemicals and reagents

MG solution (40% in H$_2$O, Sigma-Aldrich) and MTT ((3-[4,5-dimethylthiazol-2-yl]-2,5-diphenyltetrazolium bromide, Sigma-Aldrich) were purchased from Merck Life Science S.r.l.. Trypan blue (TB) solution (0.4%, Corning, Mediatech Inc, Manassas, Virginia, United States) was obtained from VWR International S.r.l. (Milan, Italy). RealTime-Glo™ MT cell viability and Caspase-Glo® 3/7 assays (Promega, Madison, Wisconsin, United States) were acquired from Promega Italia S.r.l. (Milan, Italy). Primary antibodies conjugated to Alexa Fluor®488 for MAP-2 (Merck) and fluor®594 for NSE (Santa Cruz Biotechnology, Inc., Dallas, TX, United States) were obtained from Merck Life Science S.r.l. and D.B.A. Italia S.r.l. (Segrate, Italy), respectively. Human Glo-1 (Glyoxalase I, MyBiosource) and Human HAGH (Hydroxyacylglutathione Hydrolase or Glyoxalase II, MyBiosource) ELISA Kits were obtained from CliniSciences (Guidogna Montecelio, Italy). RIPA lysis buffer (Thermo Scientific), dihydroethidium (DHE; Molecular Probes, Eugene, Oregon, United States), and Hoechst 33258 (Invitrogen) were purchased from Life Technologies Italia (Monza, Italy). Acetonitrile hypergrade for LC-MS (Sigma-Aldrich), ammonium acetate for HPLC, ≥99.0% (Fluka™, Charlotte, North Carolina, United States), 2,4-dinitrophenylhydrazine 97% (Sigma-Aldrich), MilliQ water were obtained from Merck Life Science S.r.l.

2.3 | Cell culture of hNLCs

Human primary neuronal cells were obtained from transdifferentiation of the mesenchymal stem cells (hMSCs) derived from human umbilical cord lining membranes isolated and characterized as described by Coccini et al. (2019). hMSCs were characterized based on the set of criteria proposed by the Mesenchymal and Tissue Stem Cell Committee of the ISCT (International Society for Cellular Therapy) (Bosch et al., 2012; Dominici et al., 2006). hMSCs showed a fibroblast-like shape, were plastic-adherent when maintained in standard culture conditions, and were able to differentiate into osteoblasts and adipocytes. They also showed specific surface antigen expression: about 90% of the hMSC population expressed CD105, CD73 CD90, and HLA class I, and lacked (about 10% positive) of the expression of CD34, CD45, CD14, CD31, and HLA-DR.

hMSCs were routinely cultured in 75 cm^2 flasks using MSC growth medium 2 and maintained at 37°C in a humidified atmosphere of 95% air/5% CO$_2$. hMSCs at passage (P) 3–4, according to the logarithmic growth phase, were induced to transdifferentiate into neuron-like cells using a specific protocol described by De Simone et al. (2020). Briefly, hMSCs were cultured in standard conditions until ~80% cell confluence was reached; then, the cells were detached by Accutase solution and reseeded on multiwell plates (at 4,000 cells/cm^2) coated with human fibronectin (10 μg/ml) in MSC growth medium 2. After 72 h, the whole culture medium (MSC growth medium 2) was replaced with a ready-to-use MSC neurogenic differentiation medium. The medium was changed every 48 h, and the cells were cultured up to a maximum of 8 days (fully differentiated stage).

Neuronal-like phenotype characterization was performed by morphological analysis (i.e., evidence of the conversion from the mesenchymal- to neuron-like-morphology with retractile cell bodies and long branching processes—dendrites and axons), presence of Nissl body (by staining of the granular structures of rough endoplasmic reticulum), and the expression of several neuronal-specific proteins/markers (by immunofluorescence) such as β-Tubulin III (a microtubule element of the tubulin family, structural marker predominantly in neurons), microtubule-associated protein 2 (a mature neuron marker), and enolase (cytoplasmic protein expressed by mature neurons), synaptophysin (indicator of the synapses density), growth-associated protein 43 (a key factor for axonal growth and elongation), and post-synaptic density 95 (an important scaffold protein on the post-synaptic membrane, which plays an important role in the process of synapse formation) (Coccini et al., 2022; De Simone et al., 2020).

For MTT, cell growth assay, and caspase-3/7 activity, cells were seeded into 96-well culture plates.

TB exclusion test, ROS evaluation, cell morphology evaluation, Glo-1 and Glo-2 expressions, apoptosis features, neuronal (MAP-2 and NSE) markers, and MG determination were carried out using cells seeded into six-well plates.

2.4 | Cell treatment with MG: Different concentrations at different time points (up to 48 h)

At Day 8, the hNLCs were used for the evaluation of the neurotoxic effects induced by different MG concentrations (0, 5, 10, 25, 50, 100, 200, 300, 400, and 500 μM) up to 48 h, in a single-dose, under normothermic (37°C) conditions in a humidified atmosphere of 95% air/5% CO_2. Fresh solutions of MG were prepared immediately before use by diluting MG stock solution in MSC neurogenic differentiation medium.

2.5 | Cell survival assays: MTT test–TB staining–cell growth and morphology

Neuronal cell injury was evaluated considering different parameters such as mitochondrial metabolism by MTT assay, membrane integrity by TB staining; cell viability over time by RealTime-Glo™ MT cell viability assay, and cell morphology using phase contrast microscopy.

2.5.1 | MTT assay

The tetrazolium derivatives are reduced in cells mainly by dehydrogenase enzymes, producing intracellular formazan products of specific color that can be measured photometrically after solubilization. The activity of the dehydrogenase enzymes requires NAD^+ or NADPH as co-factors and can, therefore, be seen as metabolic indicators of cell proliferation. As the result depends on mitochondrial integrity and activity, the sensitivity and general outcome of this assay are dependent on the cellular metabolic activity.

hNLCs were treated with MG (from 5 to 500 μM), and after incubation time (24 and 48 h), MTT was added to each well for 3 h (at 37°C), and thereafter, the formazan crystals formed by mitochondrial dehydrogenases were dissolved in DMSO and quantified by measuring absorbance at 550 nm (measurement) and 655 nm (reference) using a microplate reader (Bio-Rad, Segrate, Milan, Italy).

To verify the possibility of non-enzymatic reduction of MTT by MG, all experiments were paralleled by blanks containing solutions of MG (5–500 μM) in culture medium (without cells) and MTT. No difference in absorbance was observed between medium plus MG (at different concentrations) versus control (medium without MG). Data are expressed as a percentage of control.

2.5.2 | TB exclusion test

At the end of the different MG treatments (5–500 μM), after 24 and 48 h exposure, the culture media were carefully aspirated, the hNLC monolayer washed with PBS (2 ml per well), and then cells were detached from the well bottom by Accutase solution (1 ml per well for 5 min at room temperature [r.t.]). The enzymatic reaction was inactivated with the neurogenic medium (1 ml per well). Single cell suspension was obtained pipetted gently and then was collected and counted manually using Bürker chamber to determine cell viability. The cell suspension was mixed with TB 0.4% solution (in ratio of 1:10) to determine whether cells take up or exclude dye. Viable cells have a clear cytoplasm, whereas dead cells have a blue cytoplasm. Number of viable cells was determined by light microscopy as a percentage of untreated control cells.

2.5.3 | RealTime-Glo™ MT cell viability assay

To monitor over time the cell responses to MG treatment (5–500 μM), viability was also evaluated in hNLCs from 1 to 48 h by using Real Time-Glo™ MT cell viability assay, according to the protocol supplied by the manufacturer. The cell viability measurement was performed in real time: Luminescence was read after 1, 7, 24, and 48 h by Fluoroskan microplate fluorometer (Thermo Scientific) combined with PC software (Ascent Software, version 2.6, Thermo Labsystems, Helsinki, Finland).

2.5.4 | Cell morphology analysis by phase-contrast microscopy

hNLCs were monitored by using an inverted microscopy in bright field mode (equipped with a 32X phase contrast objective) to evaluate the healthy status of the cells, their growth, and morphological features, after MG (5–500 μM) treatment. Digital photographs ($n = 10$) were captured after different timepoints of treatment, such as 5, 24, and 48 h, with a camera (Canon powershot G8, Tokyo, Japan) and stored on the PC.

2.6 | Intracellular ROS detection by DHE

ROS production within the hNLCs after MG exposure were detected using DHE, a cell permeable fluorescent dye. DHE is oxidized by cytosolic ROS to fluorescent ethidium bromide, which intercalates with the nuclear DNA yielding a red fluorescence signal within the nucleus. The latter was counterstained with Hoechst 33258 blue fluorescence dye. Nuclear ethidium bromide red fluorescence intensity is proportional to ROS amount into cytoplasm.

After cell treatment with MG for 24 and 48 h, the hNLCs were incubated with DHE (5 μM) at 37°C in darkness for 30 min. Next, hNLCs were washed in PBS and fixed in 4% paraformaldehyde (PF) for 20 min at r.t., washed again with PBS, and treated with 12 μg/ml Hoechst 33258 for 15 min at 37°C and 5% CO_2 in the incubator. Finally, cells were washed again with PBS, mounted with Fluoroshield, and let dry at environmental conditions in darkness. All images were collected with the digital camera (Infinity2) combined with a fluorescence microscope (CX41 Olympus, Tokyo, Japan), provided by EPI LED Cassette (FRAEN, Settimo Milanese [MI], Italy). Digital images ($n = 6$, from each concentration and for each time point) were captured using 100X oil objective lens, and measurement conditions were the following: 470 nm excitation (T% = 40), 505 nm dichroic beamsplitter, and 510 nm long pass filter.

2.7 | Apoptosis evaluation by nuclear fluorescence staining

hNLCs cultures treated with MG (10–500 μM for 24 and 48 h) were fixed in PF 4% (20 min at r.t.), washed (PBS), and then supravitally stained with the fluorescent nuclear dye, Hoechst 33258 (5 μM for 10 min at r.t.). Afterward, hNLCs were washed again (PBS), let dry, and scored under fluorescence microscope equipped with a 40X objective. The microscopic fields were photographed and stored on PC. Apoptotic cells were quantified in different picture ($n = 6–8$ for each concentration and timepoint) and expressed as percentage of total cells counted (viable cells plus apoptotic cells) of control.

2.8 | Caspase-3/7 activity

Caspase-Glo® 3/7 assay is a luminescence-based test system that measures the caspase-3 and caspase-7 activities. Adding caspase-Glo® 3/7 Reagent in an "add-mix-measure" format, directly to the well, results in cell lysis followed by caspase cleavage of the substrate and generation of a luminescent signal, produced by luciferase, which is proportional to the amount of caspase activity present. According to the protocol supplied by the manufacturer, the caspase-3/7 activity was evaluated in hNLCs, after MG treatments 5–500 μM, for 24 and 48 h, and the luminescence signal quantified using a microplate fluorometer combined with PC software. Background luminescence (blank) associated with the culture medium used for hNLCs was determined. Then, the experimental values were obtained by subtracting the blank value.

2.9 | Glo-1 and Glo-2 activities by ELISA

Glo-1 and Glo-2 were measured using human ELISA Kits by sandwich-ELISA technique. Standards (0–100 ng/ml for Glo-1 and 0–20 ng/ml for Glo-2) and samples (control and treated with MG [25–500 μM for 24 and 48 h]) derived from cell lysates were collected following the manufacturer's instructions and then were pipetted (100 μl for each sample) into corresponding wells to bind to the antibody specific to Human Glo-1 or Glo-2 into a micro-ELISA plates. Biotinylated detection antibodies targeting human Glo-1 and Glo-2 and avidin-horseradish peroxidase (HRP) conjugate were then added successively into each well. After incubation, washing for unbound components was done. When the substrate solution was added, only wells having human Glo-1 or Glo-2, biotinylated antibody, and avidin-HRP complex were colored. The enzyme-substrate reaction was terminated by the addition of stop solution. Optical density (OD) was measured using a microspectrophotometer (BioRad) at a wavelength of 450 nm. The OD value is proportional to human Glo-1 or Glo-2 concentrations. The concentrations of Glo-1 or Glo-2 were determined by extrapolating the values on the respective standard curve.

2.10 | Expression of neuronal markers (NSE, MAP-2) by immunofluorescence analyses

Expression of NSE and MAP-2 by immunofluorescence analysis was evaluated after MG treatments (0–500 μM) at 24 and 48 h post exposure, applying the following protocol: The hNLCs were rinsed with PBS gently fixed in 4% PF (30 min at r.t.) and permeabilized with 0.1% Triton-100 (5 min at r.t.). Subsequently, the neuron-like cells were washed (twice with PBS) and blocked in PBS containing 1% bovine serum albumin (BSA; 30 min at r.t.) and finally were incubated with primary antibodies conjugated to Alexa Fluor®594 against NSE (1:100) and to Alexa Fluor®588 against MAP-2 (1:100), diluted in 1% BSA solution (60 min r.t. in dark). Next, the monolayers were washed (three times with PBS, 5 min for each washing), and the nuclei were detected using Hoechst 33258 (5 μM for 10 min at r.t.) and finally mounted with Fluoroshield.

Fluorescence images were acquired using a CX41 Olympus fluorescence microscope using 40X objective lens. The excitation conditions are described in the Section 2.6."

2.11 | MG measurement intra and extracellularly

After MG treatments (10–200 μM for 24 and 48 h), the media from each sample (control and MG treatments) were collected. Then, the hNLCs were washed with PBS (2 ml/well), detached (using Accutase solution, 500 μl/well), and harvested and counted by Burker chamber in order to normalize the cell number. After all, hNLCs (untreated and MG-treated groups) were centrifugate (2,400 rpm for 3 min) to obtain the pellet. Then, the pellets were resuspended in RIPA lysis buffer (250 μl/tube) and incubated for 15 min on ice. Finally, the lysates

were filtered using a centrifugal filter unit at 12,000g for 30 min. Media and cell lysates were stored at −20°C for later use.

MG determination in lysates and in medium samples was performed by UPLC-mass spectrometry (Waters Acquity-QDa, Waters SpA, Milan, Italy). Specifically, media and lysate samples (100 μl) underwent protein precipitation with acetonitrile (1:10) and then were vortexed and centrifugated at 13,500 rpm. An aliquot of the supernatant (200 μl) was derivatized, at 50°C for 2 h, adding 25 μl of 2,4-Dinitrophenylhydrazine (DNPH) solution (3.5 mg/ml in acetonitrile) and 275 μl of 0.5% formic acid solution in water. Afterward, samples were diluted 1:1 with Acetonitrile −10 mM ammonium acetate (50:50, v/v) and injected into the UPLC system (3 μl).

The UPLC conditions were as follows: column, Acquity BEH C18 1.7 μm (2.1 × 50 mm) at 30°C; eluent A, 10 mM ammonium acetate; and eluent B, Acetonitrile. Analysis was performed in gradient, and the cycle time was 7.5 min. The retention time of MG-DNPH was 1.7 min. The linearity of the method was assessed between 2 and 200 μM.

The MS conditions were as follows: electrospray interface in negative ion mode; single ion monitoring acquisition, m/z 250.75 (CV 5). The detection limit (signal-to-noise ratio = 3) was 0.2 μM. Reaction with DNPH leads to different derivatized compounds related to the presence of two reactive sites on MG: the acetyl and the keto group. Thus, there are two mono-derivatized and one bi-derivatized compounds. The most abundant derivative compound has been used for the determinations.

2.12 | Data analyses

Data of the cytotoxicity effects (MTT, TB, cell growth, caspase-3/7, nuclear staining, and Glo-1 and Glo-2 expression) were expressed as the mean ± SD of three separate experiments each carried out in two (TB test, nuclear staining, and Glo-1 and Glo-2 expression) or six replicates (MTT assay cell growth and caspase-3/7 activity). Statistical analysis was performed by two-way ANOVA followed by Dunnett's test post hoc test for multiple comparisons. P values less than 0.05 were considered to be significant.

The IC$_{50s}$ (50% Inhibitory Concentration) for MG were calculated from cell viability curves obtained from MTT and TB data. IC$_{50}$ determination was performed using AAT Bioquest IC$_{50}$ calculator (available on https://www.aatbio.com/tools/ic50-calculator).

3 | RESULTS

3.1 | Mitochondrial function in hNLCs after MG exposure

Mitochondrial function decreased with increasing concentrations of MG and incubation time. MG caused mitochondrial injury after 24 h exposure starting at 300 μM with about 50% cell viability decrease and further reduction (60–70% cell decrease) at the higher

concentrations tested (400–500 μM). The effects was worsened following 48 h exposure: A cell decrease (~60–85%) was observed from 300 to 500 μM (Figure 1). The MG IC$_{50s}$ were 340.46 ± 43.20 μ and 298.30 ± 37.00 μM after 24 and 48 h, respectively.

3.2 | Cell viability evaluation in hNLCs after MG exposure

Exposure of hNLCs to MG induced cell death in a concentration- and time-dependent manner (Figure 2). Significant cell viability decrease evaluated by TB test was evident from 50 μM after 24 h (~20%) and 25 μM after 48 h (~35%). Increasing concentrations of MG resulted in a significantly increased degree of cell death.

The concentrations required to inhibit (or kill) 50% of the cell population (IC$_{50}$) were 312.13 ± 42.20 μM after 24 h and 220.81 ± 35.30 μM after 48 h.

3.3 | Cell growth

A significant concentration-dependent inhibition of cell proliferation was observed from 5 to 500 μM and over time in hNLCs. The effect was significant already after 1 h exposure to MG at ≥200 μM, at ≥25 μM after 24 h, and ≥5 μM after 48 h (Figure 3).

### 3.4 | Effects of MG treatments on oxidative stress in hNLCs

The MG-induced intracellular oxidant production in hNLCs was assessed by DHE fluorescent nuclear dye, whose fluorescence intensity is directly proportional to the amount of ROS species in the cell. Redox impairment caused by MG in hNLCs is visible in Figure 4: the red fluorescence, indicating ROS generation, and increased in a concentration- and time-dependent manner (Figure 4). The effects were observed from low concentration (10 μM) after 24 h exposure, and the fluorescent red spots (generated from ROS) in the nucleus appeared markedly more evident at the higher concentrations (25–500 μM, Figure S1). The effects were exacerbated and worsened over time (Figures 4 and S1). At the higher concentration (≥200 μM), the (few) remaining live cells also showed more red spots.

Furthermore, MG at 500 μM caused a sharp hNLC density decrease at both time points.

3.5 | Apoptotic cell death in hNLCs after MG exposure

The cell death, by analyzing the nuclear outcomes, in the cells exposed to MG was evaluated by Hoechst 33258 dye (Figure 5A). The fluorescence images of the hNLCs control displayed oval-shaped blue nuclei with chromatin packaged into a single mass and

FIGURE 1 Mitochondrial function evaluation by MTT assay in hNLCs exposed to increasing concentrations (5–500 µM) of MG after 24–48 h exposure. Data are expressed as percentage of viable cells (% of control) and represent the mean ± SD. Statistical analysis by two-away ANOVA, *$P < 0.05$ different from control (Dunnett's post hoc multiple comparison test).
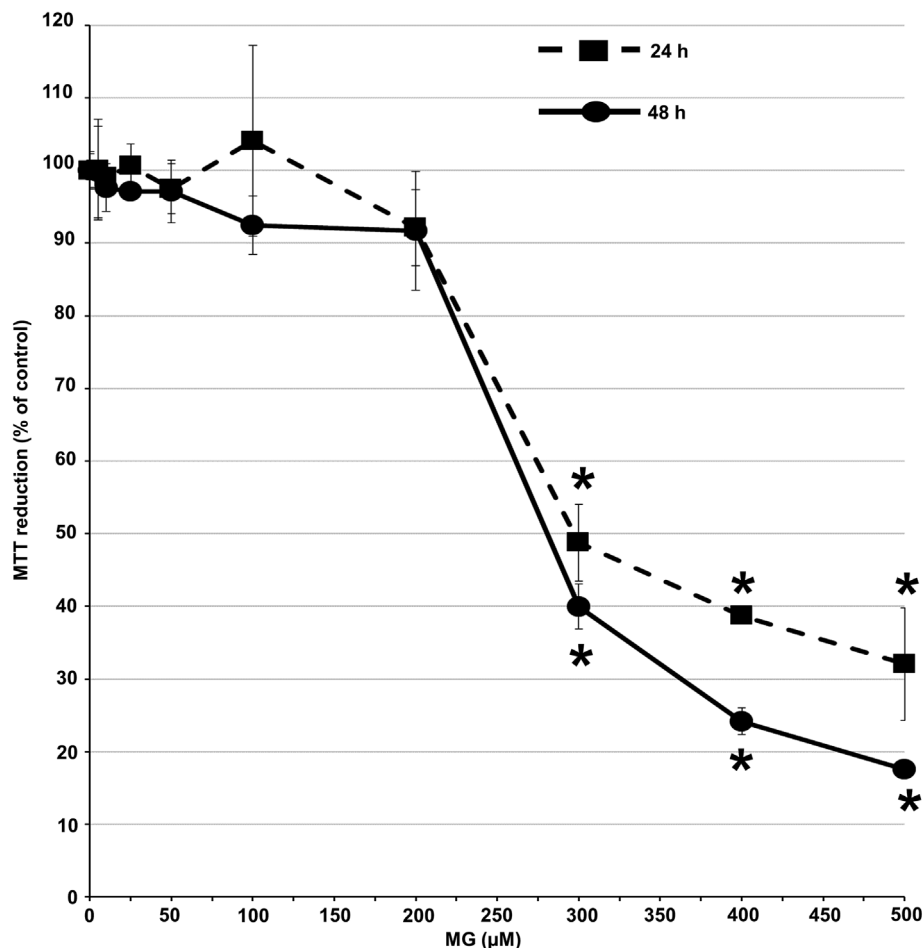
no signs of nuclear fragmentation, while MG-treated hNLCs showed typical morphological hallmarks of apoptosis in the nuclei suggestive of the MG capability to induce an apoptotic insult. Chromatin condensation and nuclear fragmentation were already detected at the lower concentration tested (10 µM) after 24 h. Exacerbation of nuclear changes including shrinkage and fragmentation of nucleus was visible at the higher concentration (300–500 µM) and prolonged exposure (48 h).

Quantitative analysis in terms of percentage of total cells, that is, viable cells plus apoptotic cells, compared to total cells of control, showed that MG induced a significant increase in the percentage of apoptotic cells (over 5%) compared to untreated hNLCs (20% apoptotic cells) already at the lowest concentration tested (10 µM) reaching a maximum effect (about +35%, respected to untreated hNLCs) at 500 µM after 24 and 48 h (Figure 5B). Altogether, these data also underlined a concentration-dependent cell density decrease (Figure 5A,B) coherently with the data obtained from the cytotoxic tests (MTT and TB).

3.6 | Caspase 3/7 activity evaluation

Upon MG treatments (5–500 µM), the hNLCs showed caspase-3/7 activation. Specifically, an elevated increase of luminescence caspase-3/7 signal was detected starting from 400 µM (+2.6-fold) after 24 h and from 200 µM (+1.2-fold) after 48 h exposure when compared to control (Figure 6).

3.7 | Morphological changes in hNLCs after MG exposure

hNLC controls adhered completely to plastic as homogeneous monolayers and maintained their typical neuronal like morphology consisting in transparent bodies, long and thin cellular processes connected into an organized network with adjacent cells (Figure 7).

Microscopic observations using phase-contrast microscopy revealed strong morphological alterations at the highest MG concentration tested (200 µM) after 5 h exposure, that is, a loss of cellular neurites, shrinkage or swelling of cell bodies and disruption of the networks, cell clusters and floating cells, cell debris as well as detachment of non-viable cells from the surface of culture plates and reduction in the number of cells, the effects persisted and worsened following exposure time (Figure 7).

The cell density decreases and morphological changes, such as cell round shape, were observed starting ≥200 µM after 5 h and 100 µM after 48 h (Figure 7). While at ≤50 µM of MG, no changes were observed (Figure S2).
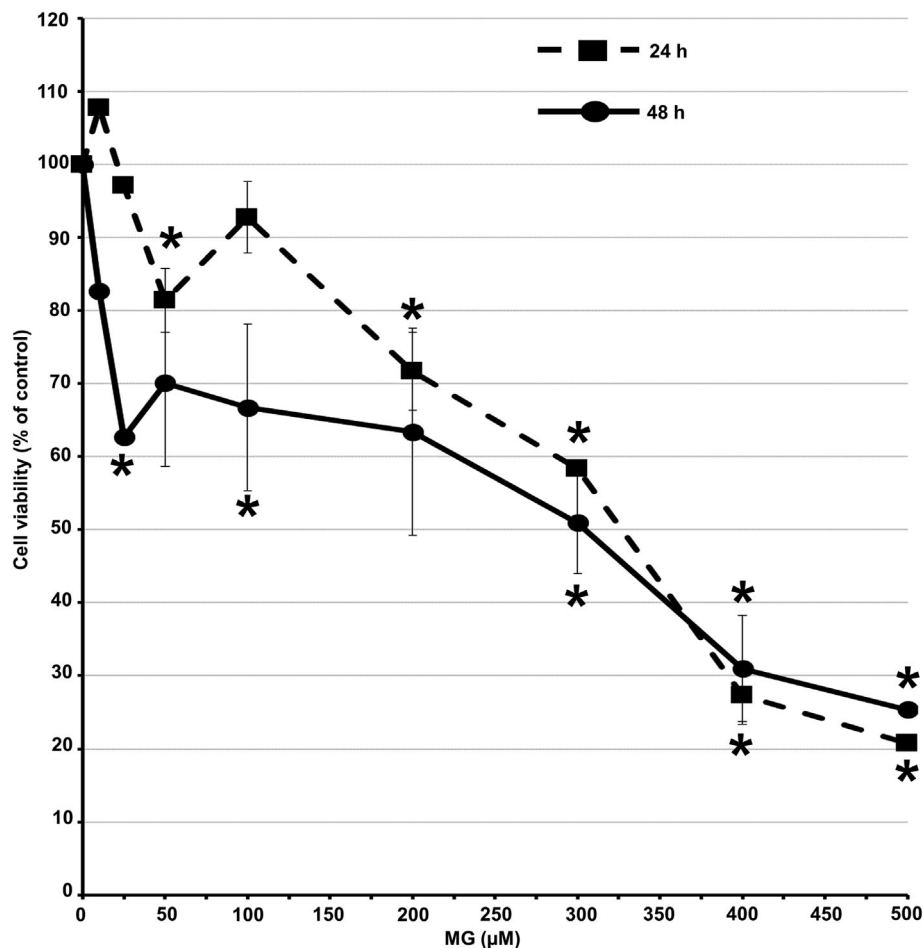
FIGURE 2 Cytotoxicity effects evaluation by Trypan blue (TB) exclusion test in hNLCs treated with increasing concentrations (10–500 μM) of MG for 24 and 48 h exposure. Data are normalized to the mean value obtained under control condition and expressed as percentage (%) of control and plotted as the mean ± SD. *$P < 0.05$, statistical analysis by two-away ANOVA followed by Dunnett's post hoc multiple comparison test.

3.8 | Determination of MG in media and cell lysates

In hNLCs, free MG levels in media ranged from 50 to 70% of the nominal concentration 1 h after addition of MG (10–200 μM). After 4 and 8 h, a sharp decrease resulted from each tested concentration although about 20–30% of free MG was still present in the media (Figure 8A).

In cell lysates, free MG level remained low (around 1.1–1.9 μM) regardless of MG concentration and independent from the elapsed time (Figure 8B).

3.9 | Glo-1 and Glo-2 evaluation

The pattern of Glo-1 in hNLCs differed between the low (25–200 μM) and the high (300 μM) MG concentrations. Specifically, Glo-1 level decreased and remained low (about 2–3-fold compared to untreated hNLCs) between 25 and 200 μM, while, in hNLCs exposed to 300 μM, Glo-1 value returned to basal level (untreated hNLCs) after 24 h. The same trend persisted after 48 h exposure (Figure 9A). Differently, Glo-2 expression significantly increased (about 10- to 39-fold compared to untreated hNLCs) after 48 h. No changes in

Glo-2 expression were detected after 24 h MG treatments (Figure 9B).

3.10 | Neuronal markers evaluation after MG exposure (NSE and MAP-2)

hNLCs exhibited a concentration- and time-dependent loss of fluorescence intensity NSE- and MAP-2-positive neurons after MG exposure (Figures 10, 11, S3, and S4). Specifically, decrease of red (NSE) fluorescence intensity was detected at 100 μM after 24 h with further exacerbation at the higher concentrations and following 48 h exposure (starting at 50 μM) (Figures 10 and S3). In addition, an increase of the apoptotic cells (with condensed nuclei) was also observed as demonstrated by Hoechst 33258 dye (see Section 3.5).

Similar pattern was observed for MAP-2 but with a greater MG-induced effect: since loss of green fluorescence intensity occurred at lower concentrations than NSE (i.e., at 25 μM vs. 100 μM after 24 h). The effects persisted and worsened at the higher MG concentrations after 48 h exposure (starting at 10 μM) (Figures 11 and S4). The apoptotic cells identified by Hoechst 33258 dye were observable even in these fluorescence pictures (see Section 3.5).

FIGURE 3 Cell growth evaluation, by RealTime-Glo™ MT cell viability assay, in hNLCs exposed to increasing MG concentration (5–500 μM) after 1, 7, 24, and 48 h. Results are provided as means ± SD. *$p < 0.05$, statistical analysis by one-way ANOVA followed by Tukey's multiple comparisons test (figure in color online).
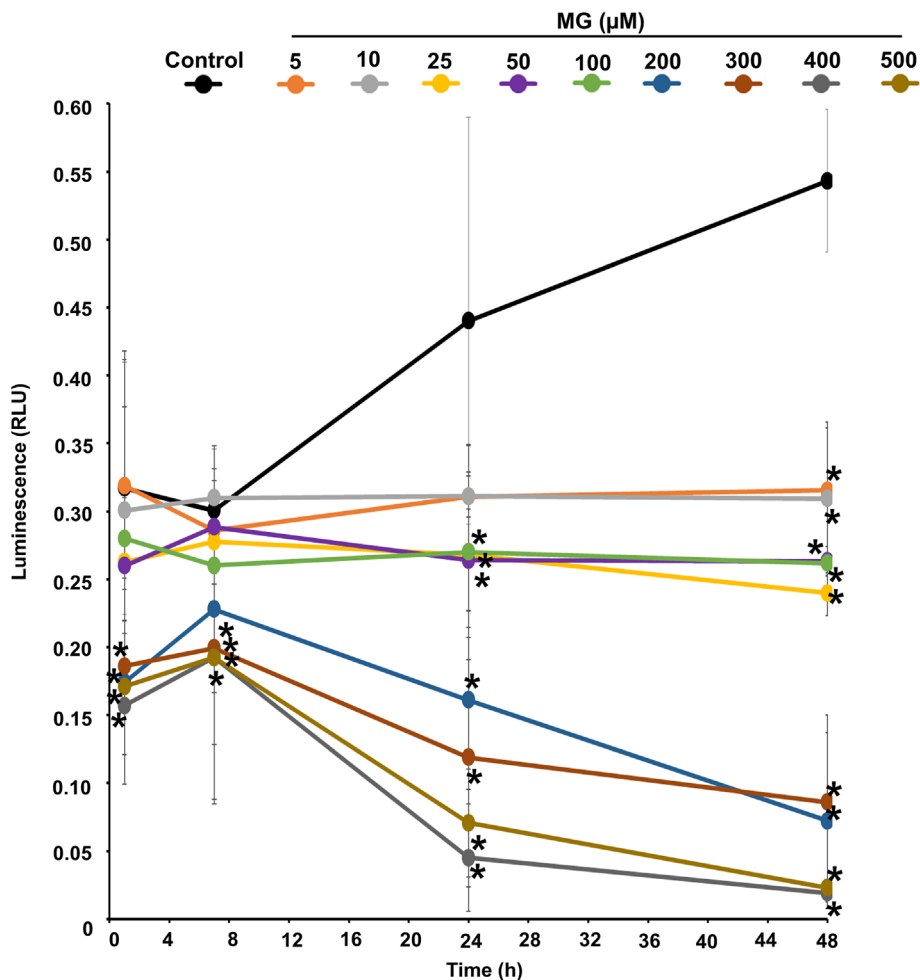

FIGURE 4 ROS evaluation. Representative images of randomly selected fluorescence microscopic fields of hNLCs treated with increasing concentrations of MG (10, 200, and 500 μM) after 24 and 48 h. DHE fluorescent dye (red) and Hoechst 33258 stain (blue) were used to detect the ROS and nucleus, respectively. Red dots were visible in the nucleus due to accumulation of oxidized DHE by ROS; the fluorescent intensity of the dots is equivalent to the relative levels of ROS present in hNLCs. Scale bar: 100 μm (figure in color online).
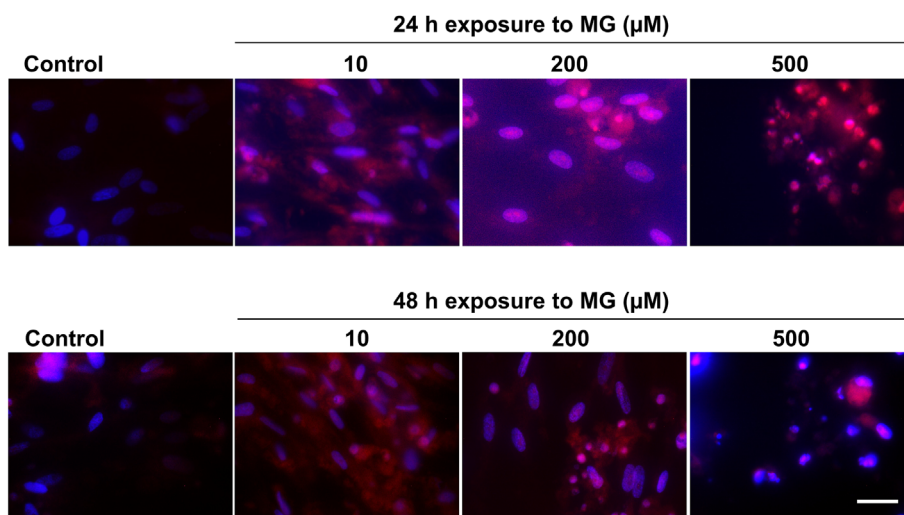
4 | DISCUSSION

The present in vitro results demonstrate the cytotoxicity induced by MG at low concentrations, on human primary neurons, and support the use of this human cell-based model as species-specific in vitro tool suitable for the evaluation of neurotoxicity induced by other dicarbonyls than MG. Remarkably, the MG-induced cytotoxicity in hNLCs occurred at concentrations approaching pathological plasma range determined in several diseases/patients (Kong et al., 2014; McLellan et al., 1994; Piazza et al., 2021).

In this model, MG increased ROS production (from 10 μM) and decreased cell viability (from 25 μM) and growth proliferation
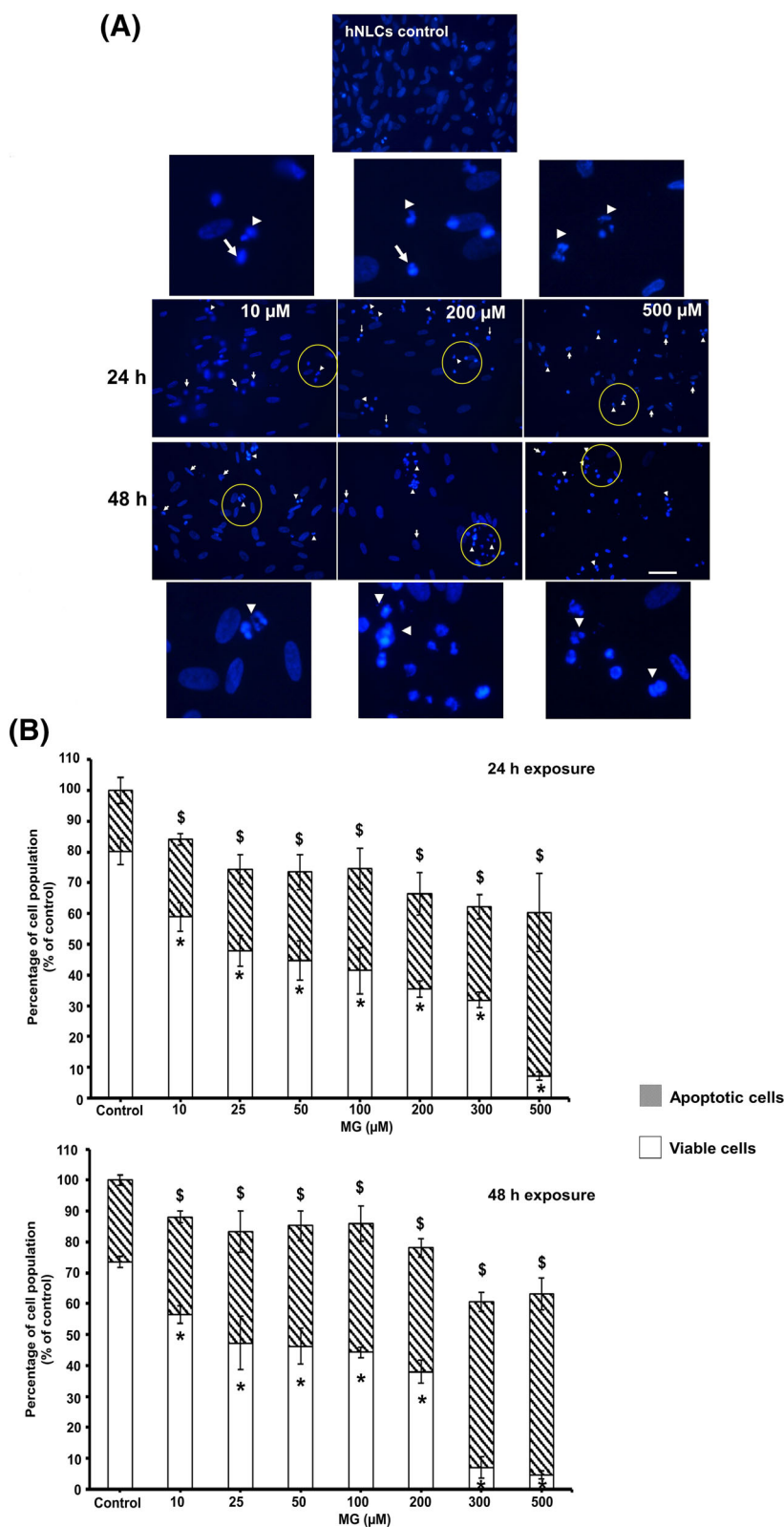
(A)

(B)

FIGURE 5   Nuclear staining. Evaluation of apoptotic features in hNLCs after MG exposure. (A) Nuclear staining using Hoechst 33258 dye: hNLCs treated with increasing concentrations of MG for 24 and 48 h showed alterations compatible with apoptotic cell hallmarks. Representative images in fluorescence microscope are taken using magnification X40; insert 2.5X. Scale bar 50 μm. Changes in nuclear morphology such as cell shrinkage, as well as chromatin condensation and fragmentation, were indicated by white arrows and white heads, respectively (figure in color online). (B) Quantitative analysis of nuclear staining in hNLCs cells. Apoptotic cells were expressed as % of total cell number, respect to the control cells. Data represent the mean ± SD. Viable cells: *$p < 0.05$, different from control (Dunnett's post hoc multiple comparison test); apoptotic cells: $^\$p < 0.05$ different from control (Dunnett's post hoc multiple comparison test).

(from 5 to 10 μM), inducing the first characteristic apoptotic effects already from low concentrations (10 μM) with important alterations of the cellular morphology starting from 100 μM, followed by even more marked effects resulting in a high number of dead cells after a few hours (5 h) from the addition of 200 μM.

Starting at MG levels of 25 μM, Glo-1 also significantly decreased while Glo-2 increased. Furthermore, MG markedly affected the neuronal markers MAP-2 and NSE causing their loss, again resulting from the exposure to low MG concentration, that is, ≥10 μM.

FIGURE 6 Caspase-3/7 activity evaluation in hNLCs treated with increasing concentrations of MG for 24 and 48 h. Upon treatment with higher concentrations (≥400 µM after 24 h and ≥200 µM after 48 h) of MG a marked increase of caspase-3/7 activity was observed. Data represent the mean ± SD. Statistical analysis by two-away ANOVA, *$p < 0.05$ different from control (Dunnett's post hoc multiple comparison test) (figure in color online).
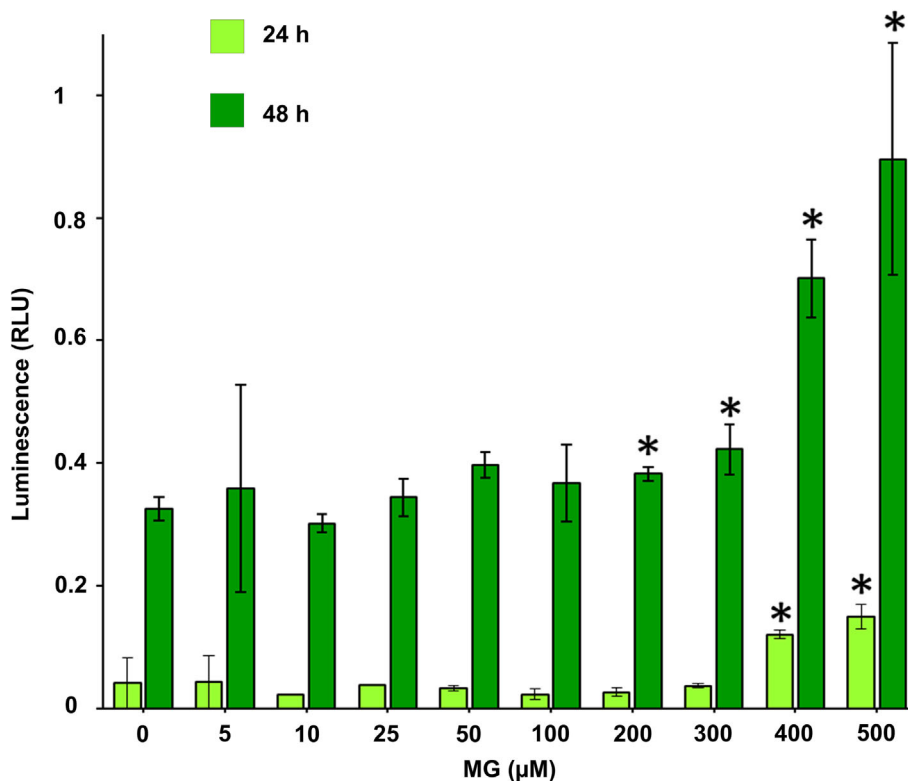
The lowest MG concentration that caused in vitro toxicological effects (i.e., reduction of growth proliferation, overproduction of intracellular ROS, induction of apoptosis, and reduction of neuronal markers) in these primary cells, hNLCs differentiated from the MSCs, was 10 µM, a concentration much lower compared to that detected in other studies applying human neuroblastoma cell lines, like SH-SY5Y, SK-N-SH, SK-N-MC, and M17, where the cytotoxic effects occurred from 250 µM up to over 800 µM (Haddad et al., 2019; Suh et al., 2022; Tajes et al., 2014). Moreover, the recent employment of human-induced pluripotent stem cells (hiPSCs)-derived neurons also evidenced neither cell death nor mitochondrial dysfunction at concentrations of MG up to 200 µM after 24 h (Hara et al., 2021). In another recent study evaluating cell survival of both human M17 neuroblastoma cells and iPSC-derived neurons after 10–10,000 µM exogenously added MG, the M17 cells showed a clear loss of viability although MG exhibited a high IC$_{50}$ (809.2 µM), while neurons derived from human iPSC line showed no loss of viability across a 10–1,000 µM MG range (Conti Mazza et al., 2022).

Overall, our findings demonstrated that human primary neurons (hNLCs) seemed more susceptible to MG exposure than both the human immortalized neuroblastoma cell lines (e.g., SH-SY5Y, SK-N-SH, SK-N-MC, and M17) and hiPSCs-derived neurons, probably for the tumor of neuron cell lines (neuroblastoma). In fact, many cancer cell lines are known to overexpress Glo-1, which may reflect a cellular response to elevated cellular MG stress associated with glycolytic adaptations of cancer cells, commonly referred to as the "Warburg effect" (Bair et al., 2010; Fantin et al., 2006; Frandsen &

Narayanasamy, 2017; Leone et al., 2021; Sakamoto et al., 2001; van Heijst et al., 2006).

The very low susceptibility or no loss of viability observed in human iPSCs-derived neurons treated with high MG concentrations may rely on the peculiar characteristics of iPSCs that specifically regulate own glycolysis for maintaining their embryonic features, as the reprogramming of "adult" differentiated somatic cells to "embryonic" pluripotent SCs is accompanied by increased rate of glycolysis. Nevertheless, glycolysis triggers accumulation of AGEs, a potential causative factor in aging, by promoting MG production demonstrating that iPSCs possess factors that, in rearranging cellular status to embryonic pluripotent state from differentiated state in the reprogramming process by clearing accumulated toxic molecules (MG and AGEs), still persist to maintain the intrinsic pluripotency (Kang et al., 2019).

In hNLCs, the low MG concentration, 10 µM, caused an overproduction of intracellular ROS after 24 h, which worsened by increased MG concentrations, and the early signs of apoptosis were also clearly visible characterized by chromatin condensation and nuclear fragmentation with exacerbation of the nuclear changes, including shrinkage and fragmentation of nucleus, evident at the higher concentrations (300–500 µM) and prolonged exposure time (48 h). The MG-induced generation of intracellular ROS at very low concentrations may be responsible for the processes leading to apoptosis with the first typical apoptotic features (morphological alterations) evident at low concentrations, while the increased caspase-3/7 was detected only at high concentration (≥200 µM) in our primary human neuronal model. Other mechanisms may probably underlie the steps leading to apoptosis. For example, in human umbilical vein endothelial cells (HUVEC,
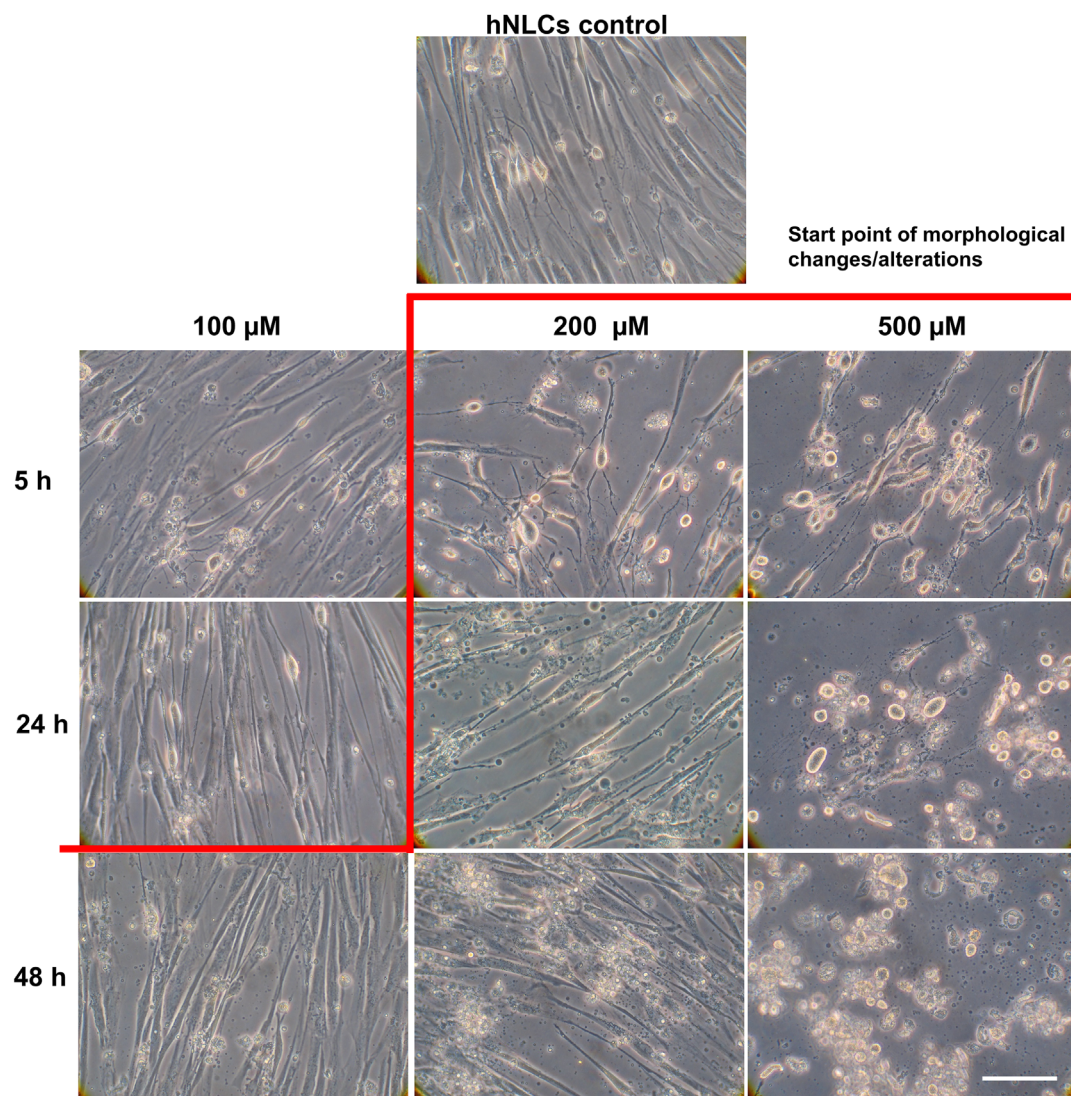
FIGURE 7 Morphological analysis under microscope. Representative photographs of hNLC morphology treated with MG for 5, 24, and 48 h. Changes/alterations in hNLC morphology were assessed using phase-contrast microscopy: Changes in cell morphology as deformation and shrinkage were apparent at 200 μM of MG after 5 h exposure, following 24 and 48 h exposure cell density decrease; floating and detached cells, as well as cluster of the round cells, were also well noticeable. Scale bar: 100 μm (figure in color online).

primary cells isolated from the vein of the umbilical cord), the ROS production after high MG concentration (i.e., 200 μM) was suggested to repress NF-kB pathways by down-regulating the p65 expression, and in turn, down-regulated the antiapoptotic c-FLIP$_L$ (a key regulator of caspase 8), leading to apoptosis in ECs (endothelial cells) (Jang et al., 2017). Again, in a recent study, 200 μM MG induced apoptosis in HUVECs partly mediated through the PI3K/Akt and Nrf2/HO-1 signaling pathways (Wang et al., 2022).

Notably, MG-induced apoptotic death was found in several cell type, that is, human umbilical vein endothelial cells (Chan & Wu, 2008), human mononuclear cells (Hsieh & Chan, 2009), SH-SY5Y neuroblastoma (Li et al., 2011), Madin-Darby canine kidney renal tubular cells (Jan et al., 2005), Neuro-2A neuroblastoma (Huang et al., 2008), Jurkat cells (Du et al., 2000), rat hippocampal (di Loreto et al., 2008), cortical neurons (Kikuchi et al., 1999), and immortalized

mouse hippocampal HT22 cells (Dafre et al., 2015), though again MG-induced toxic effects occurred at treatment doses much higher than the effective ones in hNLCs. Also, a drastic reduction of the two neuronal markers MAP-2 and NSE, indicators of the cell body, axons and neurites, and glycolytic metabolism, respectively, was induced by 10–50 μM of MG, suggesting its potential role already at low concentrations in perturbing neurite outgrowth in these cultured human primary neurons. Similar neurotoxic effects were observed in neuroblastoma cells (SK-N-SH) once more at much higher MG concentrations (500 μM) responsible of the 50% reduction of the neuronal level of NSE (Haddad et al., 2019). In laboratory animal cultured neurons, a gradual increase in dosage of MG also gradually decreased the extension of neurites (Radu et al., 2012). Moreover, a primary culture of rat hippocampal neurons, exposed to 100 μM MG, exhibited a 49% decrease in the number of MAP-2-positive neurons, and their

FIGURE 8 MG determination. MG levels were measured in media (A) and cell lysates (B) after 1, 4, and 8 h exposure to increasing concentration of MG (10–200 μM). The data are the mean of two different experiments, each carried out in triplicate (color figure online).
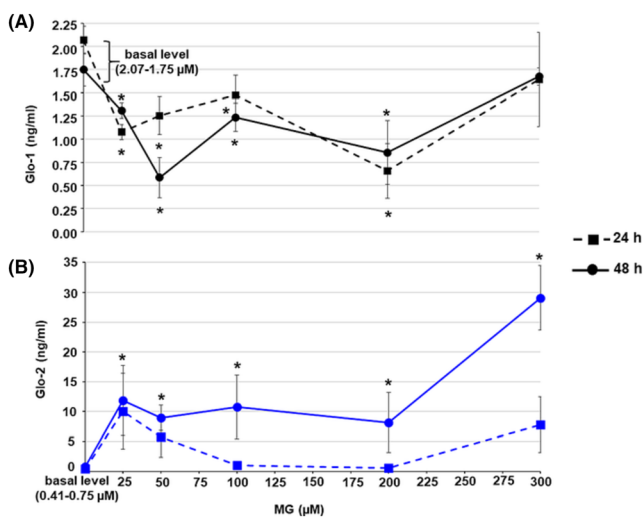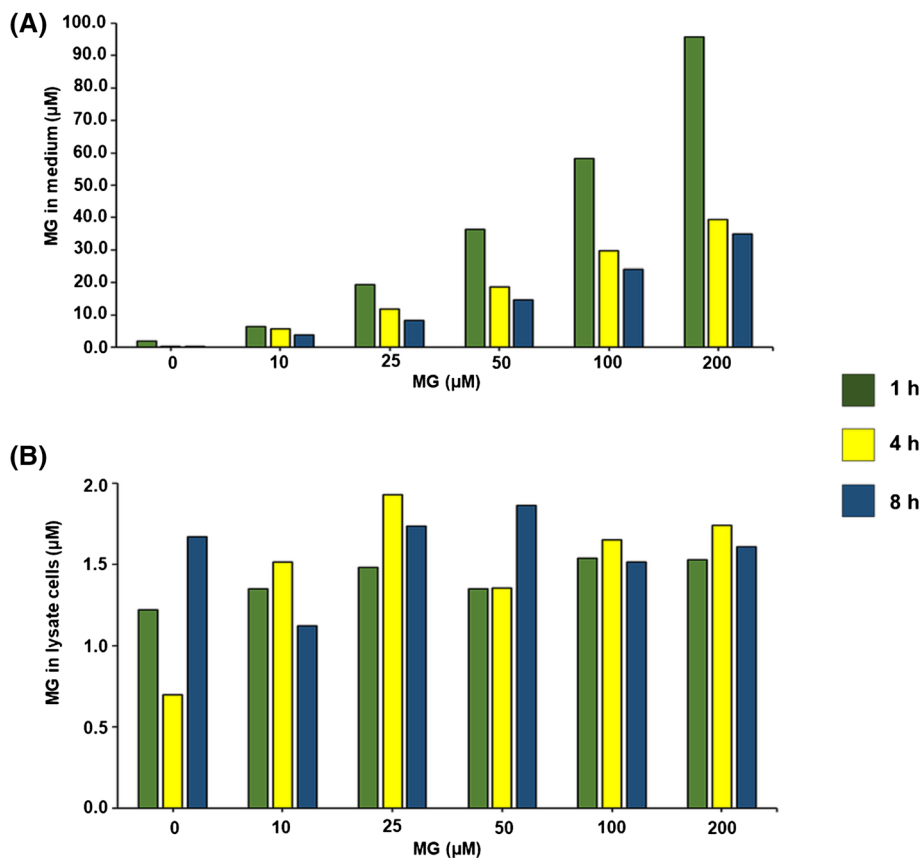

FIGURE 9 Glo-1 (A) and Glo-2 (B) evaluation in hNLCs exposed to increasing concentration of MG for 24 and 48 h. The data are expressed as mean ± SD. *$p < 0.05$, different from control (Dunnett's post hoc multiple comparison test) (figure in color online).

dendrites showed markedly retractile and tortuous appearances (Chen et al., 2010).

Due to its highly reactive electrophilic nature, a large proportion of MG covalently binds (reversible) to endogenous proteins, peptides, and amino acids (Lo et al., 1994). In physiological solutions, MG is present as unhydrated (1%) and mono- (71%) or di-hydrate (28%) forms, which are rapidly interconverted (Zheng et al., 2022). The free and reversibly bound forms of MG are in dynamic equilibrium. Moreover, there is a dynamic exchange of free MG between cellular and extracellular compartments (Rabbani & Thornalley, 2014). There is usually a negative gradient of MG concentration from the intracellular to extracellular compartments, with only enzymatic metabolism of MG inside cells. MG in the extracellular compartment of endogenous or exogenous origin enters cells for detoxification. Specifically, under normal physiological conditions, MG is efficiently scavenged mostly by the glyoxalase system. However, a minor fraction of MG, which is not metabolized/escapes detoxification, reacts rapidly with protein forming AGEs residues, and DNA to form AGEs that are thought to be the main drivers behind MG-derived cellular dysfunction involved in aging-related diseases (Ott et al., 2014; Schalkwijk & Stehouwer, 2020).

In our neuronal model (hNLCs), 1 h after addition of exogenous MG (10–200 μM), the levels of free MG in medium was about 50–70% of the nominal concentration. Over the time, after 4 and 8 h, a sharp decrease was observed for each tested concentration although about 20 to 30% of free MG was still present in medium, and after 24–48 h, the levels were very low, from 0.1 to 1.6 μM (about 1% of each initial concentration). In cell lysates, despite of MG concentration increases, free MG level remained stably low (around 1.1–1.9 μM) and independent from the elapsed time. It might be that the medium free MG enters the cells during time where is removed by the cytosolic
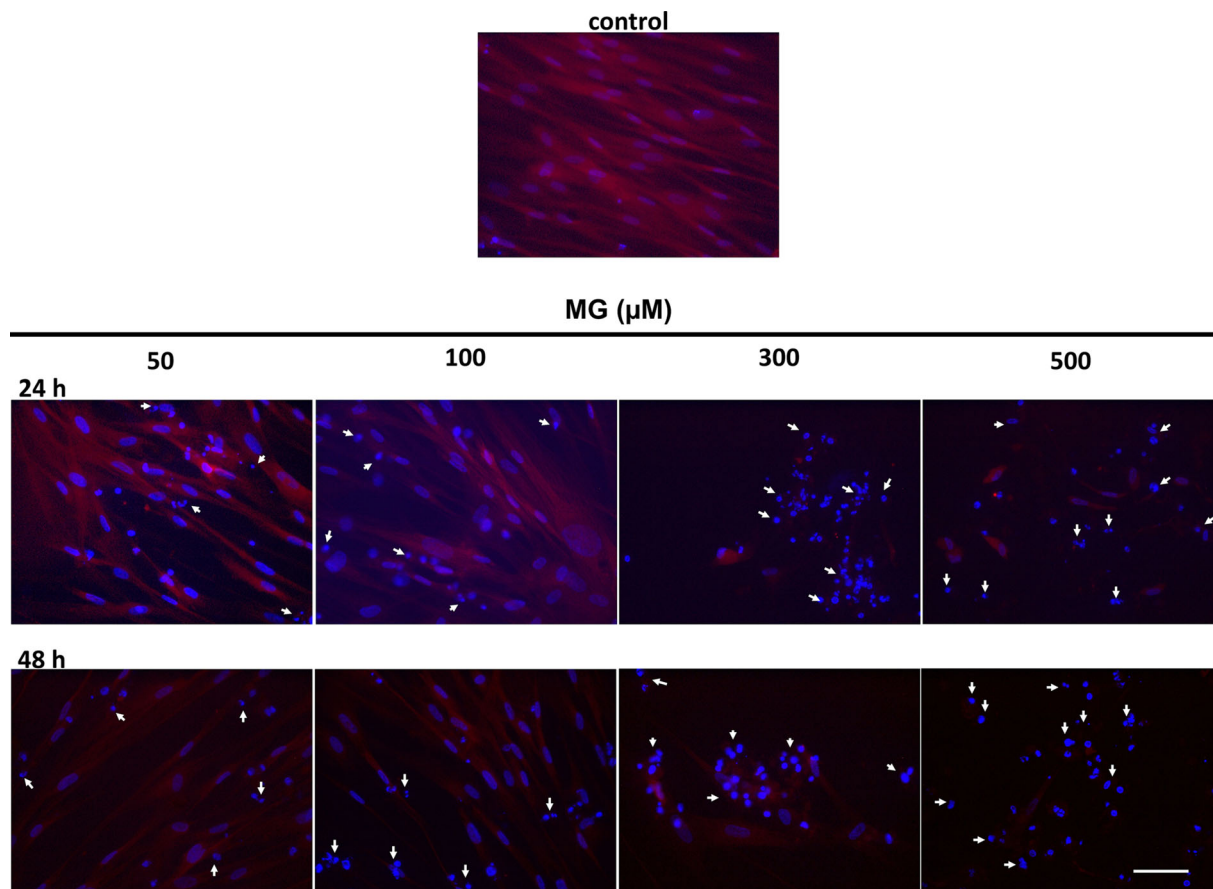
FIGURE 10 Immunofluorescence analysis of NSE after 24 and 48 h exposure to MG. Representative fluorescence merged microphotographs of hNLCs showing the MG effects on NSE expression. Nuclei were counterstained with Hoechst 33258. The fluorescence intensity decrease started from 100 μM after 24 h and 50 μM after 48 h exposure to MG with exacerbation at the higher concentrations tested combined with an increase of the condensed apoptotic cells (white arrows) detected by Hoechst 33258 dye. Scale bar: 100 μm (figure in color online).

GLO system and other minor detoxifying systems. It is known that, when the intracellular MG fraction is too high, it escapes the detoxification and immediately reacts with protein and DNA to form AGEs and cause adverse effects. The more amount of MG is added, the greater is the accumulation of AGEs in cells. In fact, regardless of the apparently cellular free MG stably low over time and uninfluenced by MG concentrations, in hNLCs, several cytotoxic effects started to be evidenced by the addition of 10 μM MG, which were exacerbated in a MG concentration- and exposure time-dependent manner. On the other hand, when the accumulation of MG exceeds the physiological cellular levels, that is, 1–4 μM, dicarbonyl stress occurs as a consequence of the imbalance between the generation/exposure and MG metabolism (Nigro et al., 2017; Scirè et al., 2022).

Moreover, in hNLCs the glyoxalase system was also affected by the addition of 25 μM MG. In particular, the Glo-1 response to MG was biphasic: At concentration between 25 and 200 μM, MG caused a decrease in Glo-1 level (24 and 48 h), followed by a rebound effect at the highest concentration tested (300 μM). A dissimilar response was observed for Glo-2: An increase of the expression was induced by MG treatments (25–300 μM) after 48 h only. The consequence of an impairment in the glyoxalase system would be an increased

susceptibility to MG. This is consistent with concentration- and time-dependent increased of cytotoxicity and oxidative stress (Bélanger et al., 2011; di Loreto et al., 2008). For instance, MG either induced or impaired the glyoxalase system in immortalized mouse hippocampal HT22 cells (Dafre et al., 2015): 300 μM MG produced an increase in Glo-2 expression at 24 h, and a decrease in Glo-1 activity after 24 h exposure to 750 μM MG. A significantly decrease of Glo-1 levels or its protein expression was also observed in several in vitro studies, and once again, this effect was induced by high MG concentrations, that is, 400 μM MG after 48 h in SK-N-MC cells (Suh et al., 2022), and 500 μM after 24 h treatment in SH-SY5Y (Tseng et al., 2019), as forecastable when using human neuroblastoma cell line. Glo-1 decrease was also observed after 8 h treatment with 2 mM MG (2–8 h) in rat INS-1 pancreatic Beta-cells (Yoo et al., 2020) and after 24 h treatment with 500 μM of MG in primary cultures of cerebellar neurons from P5 C57/BL6 mice (Frandsen & Narayanasamy, 2017).

An adequate balance between MG levels and Glo-1 activity is necessary to ensure detoxification of MG from different sources and cell survival (Nigro et al., 2017). For example, the disproportionate increase in MG to increase in glucose concentration was later
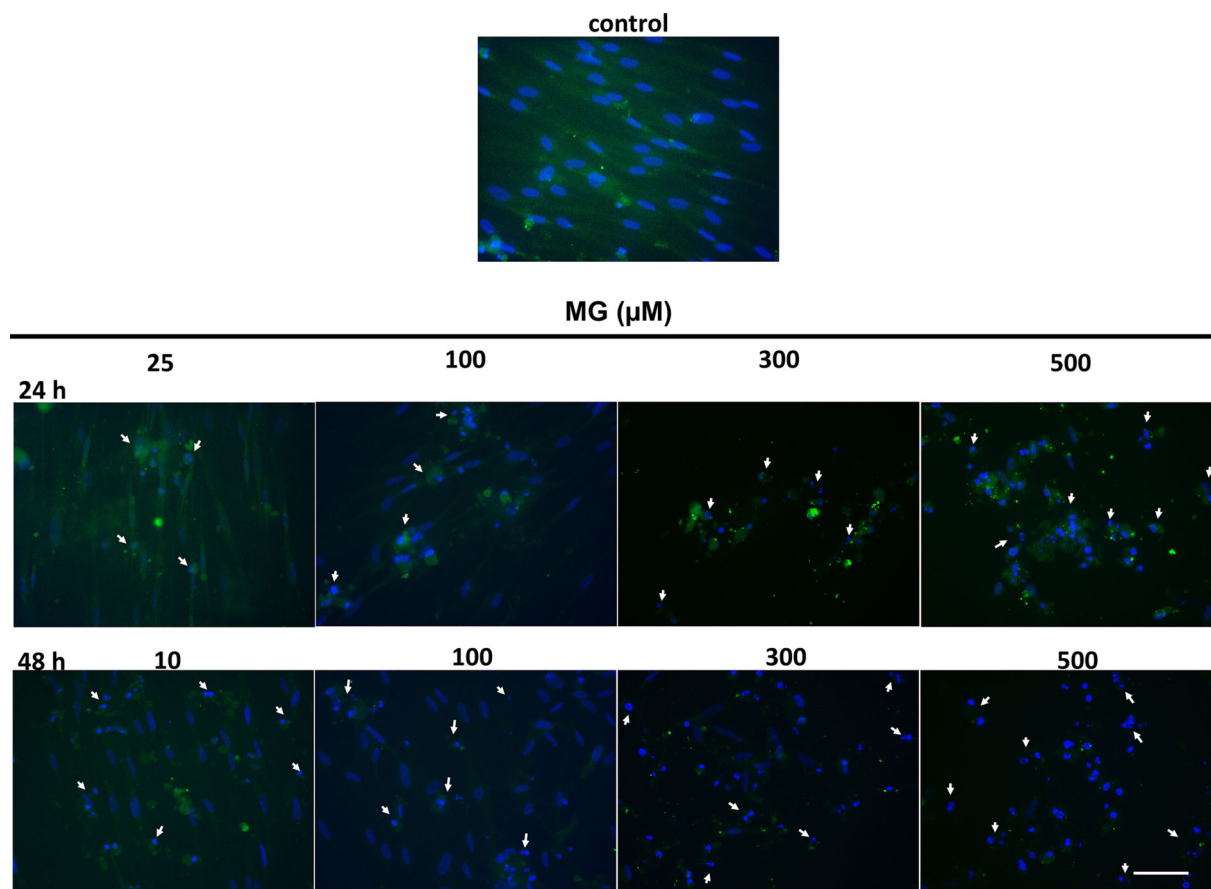
FIGURE 11   Immunofluorescence analysis of MAP-2 after 24 and 48 h exposure to MG. Representative fluorescence merged microphotographs of hNLC showing the MG effects on MAP-2 expression. Nuclei were counterstained with Hoechst 33258. The fluorescence intensity decrease started from 25 μM after 24 h and 10 μM after 48 h exposure to MG with exacerbation at the higher concentrations tested combined with an increase of the condensed apoptotic cells (white arrows) detected by Hoechst 33258 dye. Scale bar: 100 μm (figure in color online).

found to be likely due to synergistic increase in the flux of MG formation and decrease in activity of Glo-1 in tissues suffering metabolic dysfunction in hyperglycemia (Rabbani, 2022; Rabbani et al., 2016).

Noteworthy, in the present study, the lowest effective MG concentration, namely, 10 μM, is, on the other hand, more likely similar to that measured in plasma of patients with aging-related diseases, such as diabetes and AD disease, and thus clearly higher than that is expected under physiological conditions (Li et al., 2013). MG plasma concentrations in healthy individuals are around 50–500 nM and intracellular concentrations around 1–4 μM (Kold-Christensen & Johannsen, 2020; Lai et al., 2022; Rabbani & Thornalley, 2014; Scheijen & Schalkwijk, 2014).

High MG plasma levels (approaching micromolar range) can occur when the concentrations of its precursors are high, for example, in hyperglycemia, in unbalanced glucose utilization, in deficiency of TPI (triosephosphate isomerase), glycolytic enzyme, which catalyzes the conversion of dihydroxyacetone phosphate (DHAP) to glyceraldehyde-3-phosphate (G3P), thus in a TPI deficiency, the increased DHAP level leads to an accumulation of MG.

Plasma MG is from different sources, including glycated proteins formation, cells excretion, and exogenous sources (Kalapos, 2013; Maessen et al., 2015).

Under normal physiological conditions, most of plasma MG originates from in situ, whereas under pathological circumstances, such as diabetes, obesity, and AD, increased intracellular MG formation and cells outflow also increase plasma MG and thus is considered as biomarker for example for assessment of diabetic complexities because of its close relation with glycation reaction, β-cells dysfunction, obesity, and insulin resistance (Bhat et al., 2019). The increased MG levels measured in type-2 diabetes (Maessen et al., 2016) were also associated with cardiovascular disease, and markers of renal function (albuminuria) and a decline in estimated GFR (glomerular filtration rate) (Hanssen et al., 2018; Jensen et al., 2016). In type 1 diabetes, the higher plasma MG levels than those in normal subjects (i.e., 841.7 ± 237.7 and 439.3 ± 90.1 nM, respectively) significantly correlated with plasma HbA1c (glycated hemoglobin) level (Han et al., 2007). Recently, in a 2-year multicenter trial in individuals with type-2 diabetes, the plasma levels of MG measured in patients were 1,119 (907–1,590) nM (reaching more than 1 μM) (Piazza et al., 2021).

Mean plasma MG levels of 65.2 ± 19.2 ng/ml (about 1 μM) and 40.1 ± 11.1 ng/ml (0.7 μM) were reported in diagnosed type-2 diabetes subjects and controls, respectively, and MG levels correlated positively to FPG (plasma fasting glucose) and HbA1c (Kong et al., 2014).

High serum levels of MG have also been associated with increased cognitive decline in elderly subjects suggesting that an imbalance in peripheral MG metabolism may be correlated with the cause of brain pathophysiology (Beeri et al., 2011). Similar results were obtained by another study, performed in 378 participants aged between 60 and 85 years, where a higher MG serum amount was associated with poorer memory and executive function and with lower gray matter volume (Srikanth et al., 2013). The brains of patients with AD have nearly twofold higher MG levels than control individuals, with MG being 5–7 times higher in cerebrospinal fluid than in plasma (about 600 nM) (Kuhla et al., 2005; Odani et al., 1999). Likewise, AD patients have significantly higher hippocampi MG-AGEs, a finding recapitulated in the nigra neurons of PD patients (Fan et al., 2020).

Neurodegenerative diseases—including AD and PD—and aging are often induced or exacerbated by accumulation of MG (Frandsen & Narayanasamy, 2018). AD brain tissue shows high amounts of AGEs and oxidized lipids and proteins, which is a marker of inflammation (Wong et al., 2001). There is a correlation with the amount of MG/AGEs localized to specific brain regions and severity of AD (Ko et al., 2015).

Post mortem studies of PD brains show high levels of oxidized substrates and colocalization of AGEs to Lewy bodies (Dias et al., 2013).

Moreover, age, the main risk factor for AD and PD (Xie et al., 2014), is correlated with an increase in ROS formation, oxidized proteins and lipids, and apoptosis (Pisoschi & Pop, 2015) and during normal aging oxidative stress will increase while glutathione activity decreases. Glo-1 levels also drop in accordance to age, and the decrease of Glo-1 levels is strongly correlated with increasing levels of AGEs (Kuhla et al., 2006). A continuous loss of Glo-1 activity with age, such as that found in several old tissues (Haik et al., 1994; Han et al., 1976; Kuhla et al., 2006; McLellan & Thornalley, 1989; Sharma-Luthra & Kale, 1994), would lead to increased MG levels and thus trigger carbonyl stress.

Furthermore, AD is characterized by the oxidative stress generated from amyloid β-peptide (Aβ) aggregates. It produces protein nitrotyrosination, and one of the proteins more nitrotyrosinated (affected) in AD is the TPI, enzyme that plays an important role in glycolysis and is essential for efficient energy production. Nitrotyrosination of TPI (and thus TPI decrease) by Aβ is a key pathological process in AD as it triggers (increases) MG production, whose neurotoxic role involves activation of the apoptotic machinery (Tajes et al., 2014).

In summary, the present in vitro findings indicate that MG causes adverse effects on primary neuron-like cells of human origin, transdifferentiated from UC MSCs, affecting cell growth and viability, cell morphology, inducing ROS overproduction and apoptosis (apoptotic nuclei futures and caspase-3/7 activity increase), altering Glo-1 and Glo-2 enzymes for its metabolization, and markedly reducing typical neuronal markers, MAP-2 and NSE, thus perturbating neurite outgrowth.

The cytotoxic effects observed by using this human cell-based model of neurons occurred from 10 μM MG, concentrations much lower than those inducing toxicity in human neuroblastoma cell lines, animal primary cells, and human iPSCs. Remarkably, these levels approach the micromolar range detected in plasma of patients with several pathologies including diabetes, aging, and neurodegenerative diseases.

A distinct point in our study was to use a primary cell-based model of human origin for the evaluation of the mechanistic neurotoxic action induced by low doses of MG and other dicarbonyls.

Given that high MG levels (nevertheless in the low micromolar range) are effective in facilitating the pathological cascades underlying neurodegenerative disorders, due to the potent glycation of reactive dicarbonyls, such as MG, to form AGEs, which play an important role in the accumulation of amyloid β (Aβ) and neurofibrillary tangles (Angeloni et al., 2014; Li et al., 2012), it becomes imperative to further study the effects of such heterogeneous, complex group of compounds on neuronal function, by applying valuable tools, like human primary neuronal cells, as well as new in vitro models. For example, new multicellular culture models would provide more valuable information to better understand the influence of cellular crosstalk on neurotoxicity. In this context, studies using a co-culture of human primary neurons and astrocytes will help to shed light of the importance of this system in a way that is more likely to mimic human brain physiology and pathophysiology since (i) astrocytes are key players in the maintenance of brain homeostasis, (ii) astrocyte-neuron metabolic cooperation is known to shape brain activity, (iii) GLO pathway significantly differs between astrocytes and neurons in a way that renders neurons more vulnerable to MG and AGEs accumulation, and (iv), however, astrocytes being more glycolytic than neurons may help protecting neurons from MG toxicity.

The in vitro three-dimensional (3D) human neurospheres can provide an additional valuable tool, mimicking better the physiological and biochemical properties of brain tissues than the traditional two-dimensional in vitro systems (Jorfi et al., 2018; Wang et al., 2017; Yin et al., 2017). Three-dimensional spheroid model allows also for detection of adverse effects caused not only after short-term but even longer (and repeated) exposure, thus simulating chronic conditions.

Moreover, the complexity of 3D human brain organoids, multicellular aggregates form hPSCs, mimicking partially structural characteristics of the brain and neural function aspects, could provide advantages for detecting neural toxicants on large scale (Fan et al., 2022), representing a promising New Approach Method.

ACKNOWLEDGMENTS

CONFLICT OF INTEREST

The authors declare that there is no conflict of interest regarding the publication of this paper.

DATA AVAILABILITY STATEMENT

The datasets produced and/or analyzed during the present study are available from the corresponding author upon reasonable request.

ORCID

Teresa Coccini https://orcid.org/0000-0002-2039-7944
Francesca Caloni https://orcid.org/0000-0003-2527-7754

REFERENCES

Allaman, I., Bélanger, M., & Magistretti, P. J. (2015). Methylglyoxal, the dark side of glycolysis. *Frontiers in Neuroscience*, 9, 23. https://doi.org/10.3389/fnins.2015.00023

Angeloni, C., Malaguti, M., Rizzo, B., Barbalace, M. C., Fabbri, D., & Hrelia, S. (2015). Neuroprotective effect of sulforaphane against methylglyoxal cytotoxicity. *Chemical Research in Toxicology*, 28(6), 1234–1245. https://doi.org/10.1021/acs.chemrestox.5b00067

Angeloni, C., Zambonin, L., & Hrelia, S. (2014). Role of methylglyoxal in Alzheimer's disease. *BioMed Research International*, 2014, 238485. https://doi.org/10.1155/2014/238485

Bair, W. B. 3rd, Cabello, C. M., Uchida, K., Bause, A. S., & Wondraka, G. T. (2010). GLO1 overexpression in human malignant melanoma. *Melanoma Research*, 20(2), 85–96. https://doi.org/10.1097/CMR.0b013e3283364903

Beeri, M. S., Moshier, E., Schmeidler, J., Godbold, J., Uribarri, J., Reddy, S., Sano, M., Grossman, H. T., Cai, W., Vlassara, H., & Silverman, J. M. (2011). Serum concentration of an inflammatory glycotoxin, methylglyoxal, is associated with increased cognitive decline in elderly individuals. *Mechanisms of Ageing and Development*, 132(11–12), 583–587. https://doi.org/10.1016/j.mad.2011.10.007

Bélanger, M., Yang, J., Petit, J. M., Laroche, T., Magistretti, P. J., & Allaman, I. (2011). Role of the glyoxalase system in astrocyte-mediated neuroprotection. *Neuroscience*, 31(50), 18338–18352. https://doi.org/10.1523/JNEUROSCI.1249-11.2011

Bhat, L. R., Vedantham, S., Krishnan, U. M., & Rayappan, J. B. B. (2019). Methylglyoxal - An emerging biomarker for diabetes mellitus diagnosis and its detection methods. *Biosensors & Bioelectronics*, 133, 107–124. https://doi.org/10.1016/j.bios.2019.03.010

Bhat, W. F., Bhat, S. A., Khaki, P. S. S., & Bano, B. (2015). Employing in vitro analysis to test the potency of methylglyoxal in inducing the formation of amyloid-like aggregates of caprine brain cystatin. *Amino Acids*, 47(1), 135–146. https://doi.org/10.1007/s00726-014-1848-2

Bosch, J., Houben, A. P., Radke, T. F., Stapelkamp, D., Bünemann, E., Balan, P., Buchheiser, A., Liedtke, S., & Kögler, G. (2012). Distinct differentiation potential of "MSC" derived from cord blood and umbilical cord: Are cord-derived cells true mesenchymal stromal cells? *Stem Cells and Development*, 21(11), 1977–1988. https://doi.org/10.1089/scd.2011.0414

Buzanska, L., Sypecka, J., Nerini-Molteni, S., Compagnoni, A., Hogberg, H. T., del Torchio, R., Domanska-Janik, K., Zimmer, J., & Coecke, S. (2009). A human stem cell-based model for identifying adverse effects of organic and inorganic chemicals on the developing nervous system. *Stem Cells*, 27(10), 2591–2601. https://doi.org/10.1002/stem.179

Chan, W. H., & Wu, H. J. (2008). Methylglyoxal and high glucose co-treatment induces apoptosis or necrosis in human umbilical vein endothelial cells. *Journal of Cellular Biochemistry*, 103(4), 1144–1157. https://doi.org/10.1002/jcb.21489

Chen, Y. J., Huang, X. B., Li, Z. X., Yin, L. L., Chen, W. Q., & Li, L. (2010). Tenuigenin protects cultured hippocampal neurons against methylglyoxal-induced neurotoxicity. *European Journal of Pharmacology*, 645(1–3), 1–8. https://doi.org/10.1016/j.ejphar.2010.06.034

Coccini, T., De Simone, U., Roccio, M., Croce, S., Lenta, E., Zecca, M., Spinillo, A., & Avanzini, M. A. (2019). In vitro toxicity screening of magnetite nanoparticles by applying mesenchymal stem cells derived from human umbilical cord lining. *Journal of Applied Toxicology*, 39(9), 1320–1336. https://doi.org/10.1002/jat.3819

Coccini, T., Pignatti, P., Spinillo, A., & De Simone, U. (2020). Developmental neurotoxicity screening for nanoparticles using neuronlike cells of human umbilical cord mesenchymal stem cells: Example with magnetite nanoparticles. *Nanomaterials (Basel)*, 10, 1–28. https://doi.org/10.3390/nano10081607

Coccini, T., Spinillo, A., Roccio, M., Lenta, E., Valsecchi, C., & De Simone, U. (2022). Human umbilical cord mesenchymal stem cell-based in vitro model for neurotoxicity testing. *Current Protocols*, 2(4), e423. https://doi.org/10.1002/cpz1.423

Conti Mazza, M., Shuck, S. C., Lin, J., Moxley, M. A., Termini, J., Cookson, M. R., & Wilson, M. A. (2022). DJ-1 is not a deglycase and makes a modest contribution to cellular defense against methylglyoxal damage in neurons. *Journal of Neurochemistry*, 162(3), 245–261. https://doi.org/10.1111/jnc.15656

Cortés-Medina, L. V., Pasantes-Morales, H., Aguilera-Castrejon, A., Picones, A., Lara-Figueroa, C. O., Luis, E., Montesinos, J. J., Cortés-Morales, V. A., de la Rosa Ruiz, M. P., Hernández-Estévez, E., Bonifaz, L. C., Alvarez-Perez, M. A., & Ramos-Mandujano, G. (2019). Neuronal transdifferentiation potential of human mesenchymal stem cells from neonatal and adult sources by a small molecule cocktail. *Stem Cells International*, 2019, 7627148. https://doi.org/10.1155/2019/7627148

Currais, A., & Maher, P. (2012). Functional consequences of age-dependent changes in glutathione status in the brain. *Antioxidants & Redox Signaling*, 19(8), 813–822. https://doi.org/10.1089/ars.2012.4996

Czarnecka, J., Porowińska, D., Bajek, A., Hołysz, M., & Roszek, K. (2017). Neurogenic differentiation of mesenchymal stem cells induces alterations in extracellular nucleotides metabolism. *Journal of Cellular Biochemistry*, 118(3), 478–486. https://doi.org/10.1002/jcb.25664

Dafre, A. L., Goldberg, J., Wang, T., Spiegel, D. A., & Maher, P. (2015). Methylglyoxal, the foe and friend of glyoxalase and Trx/TrxR systems in HT22 nerve cells. *Free Radical Biology & Medicine*, 89, 8–19. https://doi.org/10.1016/j.freeradbiomed.2015.07.005

Dafre, A. L., Schmitz, A. E., & Maher, P. (2017). Methylglyoxal-induced AMPK activation leads to autophagic degradation of thioredoxin 1 and glyoxalase 2 in HT22 nerve cells. *Free Radical Biology & Medicine*, 108, 270–279. https://doi.org/10.1016/j.freeradbiomed.2017.03.028

de Almeida, G. R. L., Szczepanik, J. C., Selhorst, I., Cunha, M. P., & Dafre, A. L. (2023). The expanding impact of methylglyoxal on behavior-related disorders. *Progress in Neuro-Psychopharmacology & Biological Psychiatry*, 120, 110635. https://doi.org/10.1016/j.pnpbp.2022.110635

de Arriba, S. G., Stuchbury, G., Yarin, J., Burnell, J., Loske, C., & Münch, G. (2007). Methylglyoxal impairs glucose metabolism and leads to energy depletion in neuronal cells-protection by carbonyl scavengers. *Neurobiology of Aging*, 28(7), 1044–1050. https://doi.org/10.1016/j.neurobiolaging.2006.05.007

de Oliveira, M. R., Custódio de Souza, I. C., & Bittencourt Brasil, F. (2021). Promotion of mitochondrial protection by emodin in methylglyoxal-treated human neuroblastoma SH-SY5Y cells: Involvement of the AMPK/Nrf2/HO-1 Axis. *Neurotoxicity Research*, 39(2), 292–304. https://doi.org/10.1007/s12640-020-00287-w

de Oliveira, M. R., da Costa, F. G., Peres, A., & Bosco, S. M. D. (2018). Carnosic acid suppresses the H_2O_2-induced mitochondria-related bioenergetics disturbances and redox impairment in SH-SY5Y cells: Role for

Nrf2. _Molecular Neurobiology_, _55_(2), 968–979. https://doi.org/10.1007/s12035-016-0372-7

De Simone, U., Caloni, F., Gribaldo, L., & Coccini, T. (2017). Human co-culture model of neurons and astrocytes to test acute cytotoxicity of neurotoxic compounds. _International Journal of Toxicology_, _36_(6), 463–477. https://doi.org/10.1177/1091581817739428

De Simone, U., Spinillo, A., Caloni, F., Gribaldo, L., & Coccini, T. (2020). Neuron-like cells generated from human umbilical cord lining derived mesenchymal stem cells as a new in vitro model for neuronal toxicity screening: Using magnetite nanoparticles as an example. _International Journal of Molecular Sciences_, _21_(1), 271. https://doi.org/10.3390/ijms21010271

di Loreto, S., Caracciolo, V., Colafarina, S., Sebastiani, P., Gasbarri, A., & Amicarelli, F. (2004). Methylglyoxal induces oxidative stress-dependent cell injury and up-regulation of interleukin-1beta and nerve growth factor in cultured hippocampal neuronal cells. _Brain Research_, _1006_(2), 157–167. https://doi.org/10.1016/j.brainres.2004.01.066

di Loreto, S., Zimmitti, V., Sebastiani, P., Cervelli, C., Falone, S., & Amicarelli, F. (2008). Methylglyoxal causes strong weakening of detoxifying capacity and apoptotic cell death in rat hippocampal neurons. _International Journal of Biochemistry & Cell Biology_, _40_(2), 245–257. https://doi.org/10.1016/j.biocel.2007.07.019

Dias, V., Junn, E., & Mouradian, M. M. (2013). The role of oxidative stress in Parkinson's disease. _Journal of Parkinson's Disease_, _3_(4), 461–491. https://doi.org/10.3233/JPD-130230

Dominici, M., le Blanc, K., Mueller, I., Slaper-Cortenbach, I., Marini, F., Krause, D., Deans, R. J., Keating, A., Prockop, D. J., & Horwitz, E. M. (2006). Minimal criteria for defining multipotent mesenchymal stromal cells. The International Society for Cellular Therapy position statement. _Cytotherapy_, _8_(4), 315–317. https://doi.org/10.1080/14653240600855905

Dringen, R. (2000). Metabolism and functions of glutathione in brain. _Progress in Neurobiology_, _62_(6), 649–671. https://doi.org/10.1016/s0301-0082(99)00060-x

Du, J., Suzuki, H., Nagase, F., Akhand, A. A., Yokoyama, T., Miyata, T., Kurokawa, K., & Nakashima, I. (2000). Methylglyoxal induces apoptosis in Jurkat leukemia T cells by activating c-Jun N-terminal kinase. _Journal of Cellular Biochemistry_, _77_(2), 333–344. https://doi.org/10.1002/(sici)1097-4644(20000501)77:2<333::aid-jcb15>3.0.co;2-q

Fan, P., Wang, Y., Xu, M., Han, X., & Liu, Y. (2022). The application of brain organoids in assessing neural toxicity. _Frontier of Molecular Neuroscience_, _15_, 799397. https://doi.org/10.3389/fnmol.2022.799397

Fan, X., Sell, D. R., Hao, C., Liu, S., Wang, B., Wesson, D. W., Siedlak, S., Zhu, X., Kavanagh, T. J., Harrison, F. E., & Monnier, V. M. (2020). Vitamin C is a source of oxoaldehyde and glycative stress in age-related cataract and neurodegenerative diseases. _Aging Cell_, _19_(7), e13176. https://doi.org/10.1111/acel.13176

Fantin, V. R., St-Pierre, J., & Leder, P. (2006). Attenuation of LDH-A expression uncovers a link between glycolysis, mitochondrial physiology, and tumor maintenance. _Cancer Cell_, _9_(6), 425–434. https://doi.org/10.1016/j.ccr.2006.04.023

Frandsen, J., & Narayanasamy, P. (2017). Flavonoid enhances the glyoxalase pathway in cerebellar neurons to retain cellular functions. _Scientific Reports_, _7_(1), 5126. https://doi.org/10.1038/s41598-017-05287-z

Frandsen, J. R., & Narayanasamy, P. (2018). Neuroprotection through flavonoid: Enhancement of the glyoxalase pathway. _Redox Biology_, _14_, 465–473. https://doi.org/10.1016/j.redox.2017.10.015

Haddad, M., Perrotte, M., Khedher, M. R. B., Demongin, C., Lepage, A., Fülöp, T., & Ramassamy, C. (2019). Methylglyoxal and glyoxal as potential peripheral markers for MCI diagnosis and their effects on the expression of neurotrophic, inflammatory and neurodegenerative factors in neurons and in neuronal derived-extracellular vesicles. _International Journal of Molecular Sciences_, _20_(19), 4906. https://doi.org/10.3390/ijms20194906

Haik, G. M. Jr., Lo, T. W., & Thornalley, P. J. (1994). Methylglyoxal concentration and glyoxalase activities in the human lens. _Experimental Eye Research_, _59_(4), 497–500. https://doi.org/10.1006/exer.1994.1135

Han, L. P., Davison, L. M., & vander Jagt, D. L. (1976). Purification and kinetic study of glyoxalase-I from rat liver, erythrocytes, brain and kidney. _Biochimica et Biophysica Acta_, _445_(2), 486–499. https://doi.org/10.1016/0005-2744(76)90102-9

Han, Y., Randell, E., Vasdev, S., Gill, V., Gadag, V., Newhook, L. A., Grant, M., & Hagerty, D. (2007). Plasma methylglyoxal and glyoxal are elevated and related to early membrane alteration in young, complication-free patients with Type 1 diabetes. _Molecular and Cellular Biochemistry_, _305_(1–2), 123–131. https://doi.org/10.1007/s11010-007-9535-1

Hansen, F., de Souza, D. F., Silveira, S. L., Hoefel, A. L., Fontoura, J. B., Tramontina, A. C., Bobermin, L. D., Leite, M. C., Perry, M. L. S., & Gonçalves, C. A. (2012). Methylglyoxal alters glucose metabolism and increases AGEs content in C6 glioma cells. _Metabolic Brain Disease_, _27_(4), 531–539. https://doi.org/10.1007/s11011-012-9329-3

Hanssen, N. M. J., Westerink, J., Scheijen, J. L. J. M., van der Graaf, Y., Stehouwer, C. D. A., Schalkwijk, C. G., & SMART Study Group. (2018). Higher plasma methylglyoxal levels are associated with incident cardiovascular disease and mortality in individuals with Type 2 diabetes. _Diabetes Care_, _41_, 1689–1695. https://doi.org/10.2337/dc18-0159

Hara, T., Toyoshima, M., Hisano, Y., Balan, S., Iwayama, Y., Aono, H., Futamura, Y., Osada, H., Owada, Y., & Yoshikawa, T. (2021). Glyoxalase I disruption and external carbonyl stress impair mitochondrial function in human induced pluripotent stem cells and derived neurons. _Translational Psychiatry_, _11_(1), 275. https://doi.org/10.1038/s41398-021-01392-w

He, Y., Yang, Z., Pi, J., Cai, T., Xia, Y., Cao, X., & Liu, J. (2022). EGCG attenuates the neurotoxicity of methylglyoxal via regulating MAPK and the downstream signalling pathways and inhibiting advanced glycation end products formation. _Food Chemistry_, _384_, 132358. https://doi.org/10.1016/j.foodchem.2022.132358

Hernández, R., Jiménez-Luna, C., Perales-Adán, J., Perazzoli, G., Melguizo, C., & Prados, J. (2020). Differentiation of human mesenchymal stem cells towards neuronal lineage: Clinical trials in nervous system disorders. _Biomolecules & Therapeutics_, _28_(1), 34–44. https://doi.org/10.4062/biomolther.2019.065

Hsieh, M. S., & Chan, W. H. (2009). Impact of methylglyoxal and high glucose co-treatment on human mononuclear cells. _International Journal of Molecular Sciences_, _10_(4), 1445–1464. https://doi.org/10.3390/ijms10041445

Huang, S. M., Chuang, H. C., Wu, C. H., & Yen, G. C. (2008). Cytoprotective effects of phenolic acids on methylglyoxal-induced apoptosis in Neuro-2A cells. _Molecular Nutrition & Food Research_, _52_(8), 940–949. https://doi.org/10.1002/mnfr.200700360

Jan, C. R., Chen, C. H., Wang, S. C., & Kuo, S. Y. (2005). Effect of methylglyoxal on intracellular calcium levels and viability in renal tubular cells. _Cellular Signalling_, _17_(7), 847–855. https://doi.org/10.1016/j.cellsig.2004.11.007

Jang, J. H., Kim, E. A., Park, H. J., Sung, E. G., Song, I. H., Kim, J. Y., Woo, C. H., Doh, K. O., Kim, K. H., & Lee, T. J. (2017). Methylglyoxal-induced apoptosis is dependent on the suppression of c-FLIPL expression via down-regulation of p65 in endothelial cells. _Journal of Cellular and Molecular Medicine_, _21_(11), 2720–2731. https://doi.org/10.1111/jcmm.13188

Jensen, T. M., Vistisen, D., Fleming, T., Nawroth, P. P., Rossing, P., Jørgensen, M. E., Lauritzen, T., Sandbaek, A., & Witte, D. R. (2016). Methylglyoxal is associated with changes in kidney function among individuals with screen-detected Type 2 diabetes mellitus. _Diabetic Medicine_, _33_(12), 1625–1631. https://doi.org/10.1111/dme.13201

Jiang, B., Le, L., Liu, H., Xu, L., He, C., Hu, K., Peng, Y., & Xiao, P. (2016). Marein protects against methylglyoxal-induced apoptosis by activating

the AMPK pathway in PC12 cells. *Free Radical Research*, *50*(11), 1173–1187. https://doi.org/10.1080/10715762.2016.1222374

Jorfi, M., D'Avanzo, C., Kim, D. Y., & Irimia, D. (2018). Three-dimensional models of the human brain development and diseases. *Advanced Healthcare Materials*, *7*(1), 1–36. https://doi.org/10.1002/adhm.201700723

Kalapos, M. P. (2008). The tandem of free radicals and methylglyoxal. *Chemico-Biological Interactions*, *171*(3), 251–271. https://doi.org/10.1016/j.cbi.2007.11.009

Kalapos, M. P. (2013). Where does plasma methylglyoxal originate from? *Diabetes Research and Clinical Practice*, *99*(3), 260–271. https://doi.org/10.1016/j.diabres.2012.11.003

Kang, P. J., Zheng, J., Lee, G., Son, D., Kim, I. Y., Song, G., Park, G., & You, S. (2019). Glycine decarboxylase regulates the maintenance and induction of pluripotency via metabolic control. *Metabolic Engineering*, *53*, 35–47. https://doi.org/10.1016/j.ymben.2019.02.003

Kashyap, M. P., Kumar, V., Singh, A. K., Tripathi, V. K., Jahan, S., Pandey, A., Srivastava, R. K., Khanna, V. K., & Pant, A. B. (2015). Differentiating neurons derived from human umbilical cord blood stem cells work as a test system for developmental neurotoxicity. *Molecular Neurobiology*, *51*, 791–807. https://doi.org/10.1007/s12035-014-8716-7

Kikuchi, S., Shinpo, K., Moriwaka, F., Makita, Z., Miyata, T., & Tashiro, K. (1999). Neurotoxicity of methylglyoxal and 3-deoxyglucosone on cultured cortical neurons: synergism between glycation and oxidative stress, possibly involved in neurodegenerative diseases. *Journal of Neuroscience Research*, *57*(2), 280–289. https://doi.org/10.1002/(SICI)1097-4547(19990715)57:2<280::AID-JNR14>3.0.CO;2-U

Kil, K., Choi, M. Y., & Park, K. H. (2016). In vitro differentiation of human Wharton's jelly derived mesenchymal stem cells into auditory hair cells and neurons. *Journal of International Advanced Otology*, *12*, 37–42. https://doi.org/10.5152/iao.2016.1190

Kim, T. W., Che, J. H., & Yun, J. W. (2019). Use of stem cells as alternative methods to animal experimentation in predictive toxicology. *Regulatory Toxicology and Pharmacology*, *105*, 15–29. https://doi.org/10.1016/j.yrtph.2019.03.016

Ko, S. Y., Ko, H. A., Chu, K. H., Shieh, T. M., Chi, T. C., Chen, H. I., Chang, S. S., & Chang, S. S. (2015). The possible mechanism of advanced glycation end products (AGEs) for Alzheimer's disease. *PLoS ONE*, *10*(11), e0143345. https://doi.org/10.1371/journal.pone.0143345

Kold-Christensen, R., & Johannsen, M. (2020). Methylglyoxal metabolism and aging-related disease: Moving from correlation toward causation. *Trends in Endocrinology and Metabolism*, *31*(2), 81–92. https://doi.org/10.1016/j.tem.2019.10.003

Kong, X., Ma, M., Huang, K., Qin, L., Zhang, H., Yang, Z., Li, X., & Su, Q. (2014). Increased plasma levels of the methylglyoxal in patients with newly diagnosed type 2 diabetes 2. *Journal of Diabetes*, *6*(6), 535–540. https://doi.org/10.1111/1753-0407.12160

Kuhla, B., Luth, H. J., Haferburg, D., Boeck, K., Arendt, T., & Munch, G. (2005). Methylglyoxal, glyoxal, and their detoxification cation in Alzheimer's disease. *Annals of the new York Academy of Sciences*, *1043*, 211–216. https://doi.org/10.1196/annals.1333.026

Kuhla, B., Lüth, H. J., Haferburg, D., Weick, M., Reichenbach, A., Arendt, T., & Münch, G. (2006). Pathological effects of glyoxalase I inhibition in SH-SY5Y neuroblastoma cells. *Journal of Neuroscience Research*, *83*(8), 1591–1600. https://doi.org/10.1002/jnr.20838

Lai, S. W. T., Lopez Gonzalez, E. D. J., Zoukari, T., Ki, P., & Shuck, S. C. (2022). Methylglyoxal and its adducts: induction, repair, and association with disease. *Chemical Research in Toxicology*, *35*(10), 1720–1746. https://doi.org/10.1021/acs.chemrestox.2c00160

Leone, A., Nigro, C., Nicolò, A., Prevenzano, I., Formisano, P., Beguinot, F., & Miele, C. (2021). The dual-role of methylglyoxal in tumor progression—Novel therapeutic approaches. *Frontiers in Oncology*, *11*, 645686. https://doi.org/10.3389/fonc.2021.645686

Li, G., Chang, M., Jiang, H., Xie, H., Dong, Z., & Hu, L. (2011). Proteomics analysis of methylglyoxal-induced neurotoxic effects in SH-SY5Y cells. *Cell Biochemistry and Function*, *29*(1), 30–35. https://doi.org/10.1002/cbf.1714

Li, J., Liu, D., Sun, L., Lu, Y., & Zhang, Z. (2012). Advanced glycation end products and neurodegenerative diseases: Mechanisms and perspective. *Journal of the Neurological Sciences*, *317*(1–2), 1–5. https://doi.org/10.1016/j.jns.2012.02.018

Li, X. H., Du, L. L., Cheng, X. S., Jiang, X., Zhang, Y., Lv, B. L., Liu, R., Wang, J. Z., & Zhou, X. W. (2013). Glycation exacerbates the neuronal toxicity of β-amyloid. *Cell Death & Disease*, *4*(6), e673. https://doi.org/10.1038/cddis.2013.180

Lo, T. W., Selwood, T., & Thornalley, P. J. (1994). The reaction of methylglyoxal with aminoguanidine under physiological conditions and prevention of methylglyoxal binding to plasma proteins. *Biochemical Pharmacology*, *48*(10), 1865–1870. https://doi.org/10.1016/0006-2952(94)90584-3

Maessen, D. E., Hanssen, N. M., Lips, M. A., Scheijen, J. L., Willems van Dijk, K., Pijl, H., Stehouwer, C. D., & Schalkwijk, C. G. (2016). Energy restriction and Roux-en-Y gastric bypass reduce postprandial α-dicarbonyl stress in obese women with type 2 diabetes. *Diabetologia*, *59*, 2013–2017. https://doi.org/10.1007/s00125-016-4009-1

Maessen, D. E., Stehouwer, C. D., & Schalkwijk, C. G. (2015). The role of methylglyoxal and the glyoxalase system in diabetes and other age-related diseases. *Clinical Science*, *128*, 839–861. https://doi.org/10.1042/CS20140683

Manza, P., Wiers, C. E., Shokri-Kojori, E., Kroll, D., Feldman, D., Schwandt, M., Wang, G. J., Tomasi, D., & Volkow, N. D. (2020). Brain network segregation and glucose energy utilization: Relevance for age-related differences in cognitive function. *Cerebral Cortex*, *30*(11), 5930–5942. https://doi.org/10.1093/cercor/bhaa167

Masjosthusmann, S., Barenys, M., el-Gamal, M., Geerts, L., Gerosa, L., Gorreja, A., Kühne, B., Marchetti, N., Tigges, J., Viviani, B., Witters, H., & Fritsche, E. (2018). Literature review and appraisal on alternative neurotoxicity testing methods. *EFSA, External Scientific Report*, *15*(4), 1–125. https://doi.org/10.2903/sp.efsa.2018.EN-1410

McLellan, A. C., & Thornalley, P. J. (1989). Glyoxalase activity in human red blood cells fractioned by age. *Mechanisms of Ageing and Development*, *48*(1), 63–71. https://doi.org/10.1016/0047-6374(89)90026-2

McLellan, A. C., Thornalley, P. J., Benn, J., & Sonksen, P. H. (1994). Glyoxalase system in clinical diabetes mellitus and correlation with diabetic complications. *Clinical Science*, *87*(1), 21–29. https://doi.org/10.1042/cs0870021

Nigro, C., Leone, A., Raciti, G. A., Longo, M., Mirra, P., Formisano, P., Beguinot, F., & Miele, C. (2017). Methylglyoxal-glyoxalase 1 balance: The root of vascular damage. *International Journal of Molecular Sciences*, *18*(1), 188. https://doi.org/10.3390/ijms18010188

Odani, H., Shinzato, T., Matsumoto, Y., Usami, J., & Maeda, K. (1999). Increase in three alpha, beta-dicarbonyl compound levels in human uremic plasma: Specific in vivo determination of intermediates in advanced Maillard reaction. *Biochemical and Biophysical Research Communications*, *256*(1), 89–93. https://doi.org/10.1006/bbrc.1999.0221

Ott, C., Jacobs, K., Haucke, E., Navarrete Santos, A., Grune, T., & Simm, A. (2014). Role of advanced glycation end products in cellular signalling. *Redox Biology*, *2*, 411–429. https://doi.org/10.1016/j.redox.2013.12.016

Piazza, M., Hanssen, N. M. J., Persson, F., Scheijen, J. L., van de Waarenburg, M. P. H., van Greevenbroek, M. M. J., Rossing, P., Hovind, P., Stehouwer, C. D. A., Parving, H. H., & Schalkwijk, C. G. (2021). Irbesartan treatment does not influence plasma levels of the dicarbonyls methylglyoxal, glyoxal and 3-deoxyglucosone in participants with type 2 diabetes and microalbuminuria: An IRMA2 substudy. *Diabetic Medicine: Journal of the British Diabetic Association*, *38*(9), e14405. https://doi.org/10.1111/dme.14405

Pisoschi, A. M., & Pop, A. (2015). The role of antioxidants in the chemistry of oxidative stress: A review. *European Journal of Medicinal Chemistry*, *97*, 55–74. https://doi.org/10.1016/j.ejmech.2015.04.040

Popelová, A., Kákonová, A., Hrubá, L., Kuneš, J., Maletínská, L., & Železná, B. (2018). Potential neuroprotective and anti-apoptotic properties of a long-lasting stable analog of ghrelin: An in vitro study using SH-SY5Y cells. *Physiological Research/Academia Scientiarum Bohemoslovaca*, *67*(2), 339–346. https://doi.org/10.33549/physiolres.933761

Qi, L., Gao, R., Chen, Z., Lin, D., Liu, Z., Wang, L., Lin, L., Liu, X., Liu, X., & Liu, L. (2022). Liraglutide reduces oxidative stress and improves energy metabolism in methylglyoxal-induced SH-SY5Y cells. *Neurotoxicology*, *92*, 166–179. https://doi.org/10.1016/j.neuro.2022.08.007

Rabbani, N. (2022). Methylglyoxal and glyoxalase 1-a metabolic stress pathway-linking hyperglycemia to the unfolded protein response and vascular complications of diabetes. *Clinical Science*, *136*(11), 819–824. https://doi.org/10.1042/CS20220099

Rabbani, N., & Thornalley, P. J. (2014). Dicarbonyl proteome and genome damage in metabolic and vascular disease. *Biochemical Society Transactions*, *42*(2), 425–432. https://doi.org/10.1042/BST20140018

Rabbani, N., & Thornalley, P. J. (2015). Dicarbonyl stress in cell and tissue dysfunction contributing to ageing and disease. *Biochemical and Biophysical Research Communications*, *458*(2), 221–226. https://doi.org/10.1016/j.bbrc.2015.01.140

Rabbani, N., Xue, M., & Thornalley, P. J. (2016). Methylglyoxal-induced dicarbonyl stress in aging and disease: First steps towards glyoxalase 1-based treatments. *Clinical Science*, *130*(19), 1677–1696. https://doi.org/10.1042/CS20160025

Radu, B. M., Dumitrescu, D. I., Mustaciosu, C. C., & Radu, M. (2012). Dual effect of methylglyoxal on the intracellular Ca^{2+} signalling and neurite outgrowth in mouse sensory neurons. *Cellular and Molecular Neurobiology*, *32*(6), 1047–1057. https://doi.org/10.1007/s10571-012-9823-5

Sakamoto, H., Mashima, T., Sato, S., Hashimoto, Y., Yamori, T., & Tsuruo, T. (2001). Selective activation of apoptosis program by S-p-bromobenzylglutathione cyclopentyl diester in glyoxalase I-overexpressing human lung cancer cells. *Clinical Cancer Research*, *7*, 2513–2518.

Schalkwijk, C. G., & Stehouwer, C. D. A. (2020). Methylglyoxal, a highly reactive dicarbonyl compound, in diabetes, its vascular complications, and other age-related diseases. *Physiological Reviews*, *100*(1), 407–461. https://doi.org/10.1152/physrev.00001.2019

Scheijen, J. L., & Schalkwijk, C. G. (2014). Quantification of glyoxal, methylglyoxal and 3-deoxyglucosone in blood and plasma by ultra performance liquid chromatography tandem mass spectrometry: Evaluation of blood specimen. *Clinical Chemistry and Laboratory Medicine*, *52*(1), 85–91. https://doi.org/10.1515/cclm-2012-0878

Schmitz, A. E., de Souza, L. F., dos Santos, B., Maher, P., Lopes, F. M., Londero, G. F., Klamt, F., & Dafre, A. L. (2017). Methylglyoxal-induced protection response and toxicity: Role of glutathione reductase and thioredoxin systems. *Neurotoxicity Research*, *32*(3), 340–350. https://doi.org/10.1007/s12640-017-9738-5

Scirè, A., Cianfruglia, L., Minnelli, C., Romaldi, B., Laudadio, E., Galeazzi, R., Antognelli, C., & Armeni, T. (2022). Glyoxalase 2: Towards a broader view of the second player of the glyoxalase system. *Antioxidants (Basel, Switzerland)*, *11*(11), 2131. https://doi.org/10.3390/antiox11112131

Shahbazi, A., Safa, M., Alikarami, F., Kargozar, S., Asadi, M. H., Joghataei, M. T., & Soleimani, M. (2016). Rapid induction of neural differentiation in human umbilical cord matrix mesenchymal stem cells by camp-elevating agents. *International Journal of Molecular and Cellular Medicine*, *5*(3), 167–177.

Sharma-Luthra, R., & Kale, R. K. (1994). Age related changes in the activity of the glyoxalase system. *Mechanisms of Ageing and Development*, *73*(1), 39–45. https://doi.org/10.1016/0047-6374(94)90036-1

Shi, Y., Nan, C., Yan, Z., Liu, L., Zhou, J., Zhao, Z., & Li, D. (2018). Synaptic plasticity of human umbilical cord mesenchymal stem cell differentiating into neuron-like cells in vitro induced by edaravone.

Stem Cells International, *2018*, 5304279. https://doi.org/10.1155/2018/5304279

Singh, A. K., & Kashyap, M. P. (2016). An overview on human umbilical cord blood stem cell-based alternative in vitro models for developmental neurotoxicity assessment. *Molecular Neurobiology*, *53*, 3216–3226. https://doi.org/10.1007/s12035-015-9202-6

Singh, S., Srivastava, A., Kumar, V., Pandey, A., Kumar, D., Rajpurohit, C. S., Khanna, V. K., Yadav, S., & Pant, A. B. (2016). Stem cells in neurotoxicology/developmental neurotoxicology: Current scenario and future prospects. *Molecular Neurobiology*, *53*(10), 6938–6949. https://doi.org/10.1007/s12035-015-9615-2

Srikanth, V., Westcott, B., Forbes, J., Phan, T. G., Beare, R., Venn, A., Pearson, S., Greenaway, T., Parameswaran, V., & Münch, G. (2013). Methylglyoxal, cognitive function and cerebral atrophy in older people. *Journals of Gerontology*, *68*(1), 68–73. https://doi.org/10.1093/gerona/gls100

Strom, A., Strassburger, K., Schmuck, M., Shevalye, H., Davidson, E., Zivehe, F., Bönhof, G., Reimer, R., Belgardt, B. F., Fleming, T., Biermann, B., Burkart, V., Müssig, K., Szendroedi, J., Yorek, M. A., Fritsche, E., Nawroth, P. P., Roden, M., Ziegler, D., & GDS Group. (2021). Interaction between magnesium and methylglyoxal in diabetic polyneuropathy and neuronal models. *Molecular Metabolism*, *43*, 101114. https://doi.org/10.1016/j.molmet.2020.101114

Suh, K. S., Chon, S., Jung, W. W., & Choi, E. M. (2022). Protective effects of sciadopitysin against methylglyoxal-induced degeneration in neuronal SK-N-MC cells. *Journal of Applied Toxicology*, *42*(2), 274–284. https://doi.org/10.1002/jat.4211

Suma, R. N., & Mohanan, P. V. (2015). Stem cells, a new generation model for predictive nanotoxicological assessment. *Current Drug Metabolism*, *16*, 932–939. https://doi.org/10.2174/1389200216666151015113720

Szczepanik, J. C., de Almeida, G. R. L., Cunha, M. P., & Dafre, A. L. (2020). Repeated methylglyoxal treatment depletes dopamine in the prefrontal cortex, and causes memory impairment and depressive-like behavior in mice. *Neurotoxicity Research*, *45*(2), 354–370. https://doi.org/10.1007/s11064-019-02921-2

Tajes, M., Eraso-Pichot, A., Rubio-Moscardo, F., Guivernau, B., Bosch-Morato, M., Valls-Comamala, V., & Munoz, F. J. (2014). Methylglyoxal reduces mitochondrial potential and activates Bax and caspase-3 in neurons: Implications for Alzheimer's disease. *Neuroscience Letters*, *580*, 78–82. https://doi.org/10.1016/j.neulet.2014.07.047

Thornalley, P. J. (2008). Protein and nucleotide damage by glyoxal and methylglyoxal in physiological systems-role in ageing and disease. *Drug Metabolism and Drug Interactions*, *23*(1–2), 125–150. https://doi.org/10.1515/dmdi.2008.23.1-2.125

Tseng, Y. T., Tsai, Y. H., Fülöp, F., Chang, F. R., & Lo, Y. C. (2019). 2-iodo-4′-Methoxychalcone attenuates methylglyoxal-induced neurotoxicity by activation of GLP-1 receptor and enhancement of neurotrophic signal, antioxidant defense and glyoxalase pathway. *Molecules*, *24*(12), 2249. https://doi.org/10.3390/molecules24122249

Twarda-Clapa, A., Olczak, A., Białkowska, A. M., & Koziołkiewicz, M. (2022). Advanced glycation end-products (AGEs): Formation, chemistry, classification, receptors, and diseases related to AGEs. *Cell*, *11*(8), 1312. https://doi.org/10.3390/cells11081312

van Heijst, J. W., Niessen, H. W., Musters, R. J., Hinsbergh, V. W., Hoekman, K., & Schalkwijk, C. G. (2006). Argpyrimidine modified heat shock protein 27 in human non-small cell lung cancer: A possible mechanism for evasion of apoptosis. *Cancer Letters*, *241*, 309–319. https://doi.org/10.1016/j.canlet.2005.10.042

Wang, G., Wang, Y., Yang, Q., Xu, C., Zheng, Y., Wang, L., Wu, J., Zeng, M., & Luo, M. (2022). Metformin prevents methylglyoxal-induced apoptosis by suppressing oxidative stress in vitro and in vivo. *Cell Death & Disease*, *13*(1), 29. https://doi.org/10.1038/s41419-021-04478-x

Wang, Z., Wang, S. N., Xu, T. Y., Miao, Z. W., Su, D. F., & Miao, C. Y. (2017). Organoid technology for brain and therapeutics research. *CNS Neuroscience & Therapeutics*, *23*(10), 771–778. https://doi.org/10.1111/cns.12754

Wong, A., Lüth, H. J., Deuther-Conrad, W., Dukic-Stefanovic, S., Gasic-Milenkovic, J., Arendt, T., & Münch, G. (2001). Advanced glycation end-products co-localize with inducible nitric oxide synthase in Alzheimer's disease. *Brain Research*, *920*(1–2), 32–40. https://doi.org/10.1016/s0006-8993(01)02872-4

Xie, B., Lin, F., Peng, L., Ullah, K., Wu, H., Qing, H., & Deng, Y. (2014). Methylglyoxal increases dopamine level and leads to oxidative stress in SH-SY5Y cells. *Acta Biochimica et Biophysica Sinica*, *46*(11), 950–956. https://doi.org/10.1093/abbs/gmu094

Yang, Z., Zhang, W., Lu, H., & Cai, S. (2022). Methylglyoxal in the brain: From glycolytic metabolite to signalling molecule. *Molecules*, *27*(22), 7905. https://doi.org/10.3390/molecules27227905

Yin, X., Mead, B. E., Helia, S., Langer, R., Karp, J. M., & Levy, O. (2017). Stem cell organoid engineering. *Cell Stem Cell*, *18*(1), 25–38. https://doi.org/10.1016/j.stem.2015.12.005

Yoo, H. J., Hong, C. O., Ha, S. K., & Lee, K. W. (2020). Chebulic acid prevents methylglyoxal-induced mitochondrial dysfunction in INS-1 pancreatic β-cells. *Antioxidants*, *9*(9), 771. https://doi.org/10.3390/antiox9090771

Zakrzewski, W., Dobrzyński, M., Szymonowicz, M., & Rybak, Z. (2019). Stem cells: Past, present, and future. *Stem Cell Research & Therapy*, *10*(1), 68. https://doi.org/10.1186/s13287-019-1165-5

Zheng, L., van Dongen, K. C. W., Bakker, W., Miro Estruch, I., & Rietjens, I. M. C. M. (2022). The influence of intracellular glutathione levels on the induction of Nrf2-mediated gene expression by α-dicarbonyl precursors of advanced glycation end products. *Nutrients*, *14*(7), 1364. https://doi.org/10.3390/nu14071364

Zychowicz, M., Dziedzicka, D., Mehn, D., Kozlowska, H., Kinsner-Ovaskainen, A., Stępień, P. P., Rossi, F., & Buzanska, L. (2014). Developmental stage dependent neural stem cells sensitivity to methylmercury chloride on different biofunctional surfaces. *Toxicology in Vitro*, *28*(1), 76–87. https://doi.org/10.1016/j.tiv.2013.06.023

SUPPORTING INFORMATION

Additional supporting information can be found online in the Supporting Information section at the end of this article.